Islamic University of Technology

Department of Mechanical and Production Engineering

CFD MODELLING OF H-DARRIEUS VERTICAL AXIS WIND TURBINE

A Thesis by

Morium Mannan Tonni

Submitted in Partial Fulfillment

of the Requirements

for the Degree of

Bachelor of Science in Mechanical Engineering

May (2022)

CFD MODELLING OF H-DARRIEUS VERTICAL AXIS WIND TURBINE

MORIUM MANNAN TONNI

STUDENT ID: 170011015

ACADEMIC YEAR: 2020-2021

Submitted in Partial Fulfillment

of the Requirements

for the Degree of

Bachelor of Science in Mechanical Engineering

DEPARTMENT OF MECHANICAL AND PRODUCTION ENGINEERING

May (2022)

CERTIFICATE OF RESEARCH

This thesis titled "CFD MODELLING OF H-DARRIEUS VERTICAL AXIS WIND TURBINE" submitted by MORIUM MANNAN TONNI (170011015) has been accepted as satisfactory in partial fulfillment of the requirement for the Degree of Bachelor of Science in Mechanical Engineering.

——————————————————————————

Dr. Md. Rezwanul Karim (*Supervisor)*

Associate Professor

Department of Mechanical and Production Engineering (MPE)

——————————————————————————

Mr. Tahsin Sejat Saniat (*Co-Supervisor)*

Lecturer

Department of Mechanical and Production Engineering (MPE)

——————————————————————————

Dr. Md. Anayet Ullah Patwari (*Head of the Department)*

Professor

Department of Mechanical and Production Engineering (MPE)

Islamic University of Technology (IUT)

DECLARATION

I hereby declare that this thesis entitled "CFD MODELLING OF H-DARRIEUS VERTICAL AXIS WIND TURBINE" is an authentic report of study carried out as requirement for the award of degree B.Sc. (Mechanical Engineering) at Islamic University of Technology, Gazipur, Dhaka, under the supervision of Dr. Md. Rezwanul Karim, Associate Professor, MPE, IUT and Mr. Tahsin Sejat Saniat, lecturer, MPE, IUT in the academic year 2021-2022

The matter embodied in this thesis has not been submitted in part or full to any other institute for award of any degree.

_____

Morium Mannan Tonni

Student ID: 170011015

ACKNOWLEDGMENTS

In the Name of Allah, the Most Beneficent, the Most Merciful

Morium Mannan Tonni
Gazipur, May 2022

ABSTRACT

With the progress of time, as fossil fuel is being exhausted, renewable energy resources are getting more attention for their promising impact on the environment and its capability to replenish and sustainability. Wind energy is one of the most important renewable energy sources. A study shows that installed wind capacity increases by more than 30% every year. Design improvement of wind turbines has many parameters to consider for optimization. Experimental analysis is complex and not always feasible. But numerical simulation has the ability to analyze different parameters with less complexity. In this thesis, a 2D CFD simulation of an H-Darrieus vertical axis wind turbine is done. Prior to the simulation, mesh independent and time independent study was done not only to validate the result but also to reduce the computational effort. Sliding Mesh model approach was used for simulation which takes into account the vortices generated by the blades passing upwind on the blades downstream unlike over-simplified Moving Reference Frame (MRF) model. The transition SST model was used as the turbulence model which utilizes the advantages of both k-ε and k-ω models, providing better simulation results. From the simulation results, a Power co-efficient (C_p) vs Tip speed ratio λ curve was obtained and was validated against existing experimental data available in the literature. The knowledge obtained from this thesis can lead to the development of improved 2D simulations and ultimately 3D simulations in the future. This can also be used for design optimization and performance study of wind turbines.

KEYWORDS: H- Darrieus, Vertical Axis Wind Turbine, CFD Modelling, Sliding Mesh Model, Transition SST model,   Simulation, ANSYS , Fluent

TABLE OF CONTENTS

LIST OF FIGURES

LIST OF TABLES

NOMENCLATURE

MRF	Moving Reference Frame
VAWT	Vertical Axis Wind Turbine
HAWT	Horizontal Axis Wind Turbine
CFD	Computational Fluid Dynamics
DMST	Double-Multiple Stream Tube
VPM	Vortex Panel Model
AoA	Angle of Attack
RANS	Reynolds Averaged Navier Stokes
URANS	Unstable Reynolds Averaged Navier Stokes
SA	Spalart- Allmaras
FVM	Finite Volume Method
PDE	Partial Differential Equation
BC	Boundary condition
GE	Governing Equations
TSR	Tip Speed Ratio
C_p	Power Co-efficient
CAD	Computer-Aided design
A	Area
$C\mu$	Dimensionless Constant
E	Energy
F	Force
g	Gravitational acceleration
h	Height
h_o	Specific total enthalpy
i	Internal energy
k	Turbulent kinetic energy
M	Mass
N	Rotational speed
P	Power

P_k	Turbulence production
R	Radius

CHAPTER 1: INTRODUCTION

1.1 RENEWABLE ENERGY SITUATION IN BANGLADESH

The global energy demand, which is ever increasing, has risen sharply in the recent years. The developing countries' demand tops in this list. The developing countries like Bangladesh are now looking for cleaner means to cope up with this demand. At present, Bangladesh shares only 3% of renewable energy out of the total energy ratio [1]. However, Bangladesh has taken master plans to develop in the renewable energy sector. At present, one-third of this power production depends on imported fossil fuel which is expensive. About 65% of power generation depends on natural gas reserve of the country which is a source on the verge of exhaustion. Under this circumstances, the adoption of renewable energy sources for fulfilling the present and future demand is inevitable.

Table 1: The present electricity scenario of Bangladesh [2], [3], [4]

Statistics	2020-2021
Access to Electricity	99.5%
Power Generation Capacity	22031 MW
Distribution Line	612310 km
Number of consumers	21 lacs post-paid customers
Per Capita Power Generation	475 kWh
Transmission Line	12835 circuit km
Distribution System Loss	6.6%

The primary source of energy in Bangladesh is gas, which provides 65% of total energy consumption. After that, heavy fuel, high-speed diesel, and coal provide 18%, 7 % and 2%, respectively. Bangladesh imports around 5% of its total energy consumption from nearby countries. Renewable energy provides only 3% of the total energy in Bangladesh. Energy consumptions based on fuel type are shown in Figure 1. Bangladesh has around 9200 kilometers of transmission lines and 332,000 kilometers of distribution lines. The growth of electricity generation and distribution lines was around 10% in 2016 [5].

INSTALLED CAPACITY AS ON FEBRUARY, 2020
(BY FUEL TYPE)
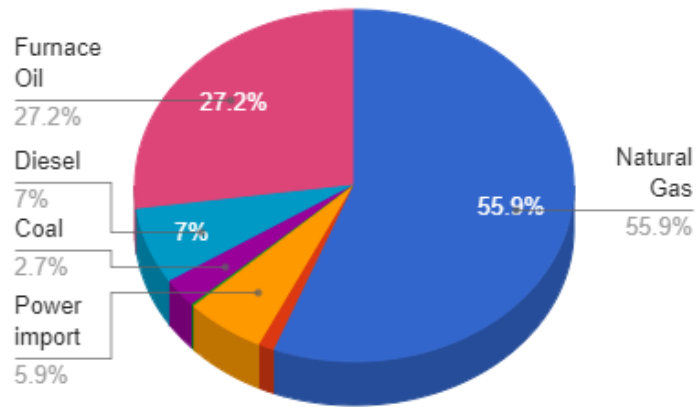
Figure 1: Primary energy consumption pattern (based on fuel types) in Bangladesh [87]
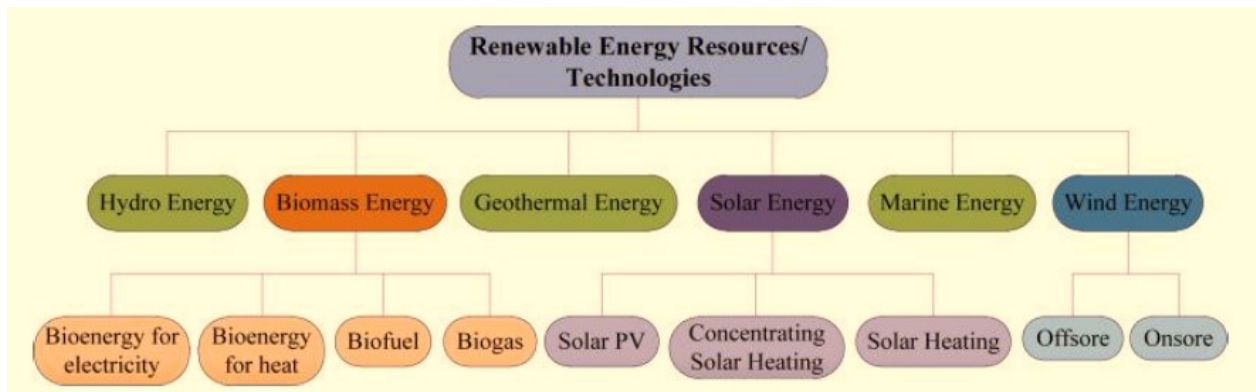
Figure 2: Renewable energy sources and technologies overview [6]

In Bangladesh, the main sources of renewable energy are solar energy, hydro energy and wind energy. Of these, 60% of total renewable energy comes from hydro energy alone. Similarly, for solar this number is 39.5% and for wind energy it is about 0.5%. Hence, it can be seen that the hydro energy is the main source of renewable energy in Bangladesh. However, the solar energy is now the fastest growing energy sector in Bangladesh and huge projects are undertaken to install solar panels both in urban, rural and remote areas of Bangladesh [7]. Figure 2 depicts the entire renewable energy sources and technologies. [6].
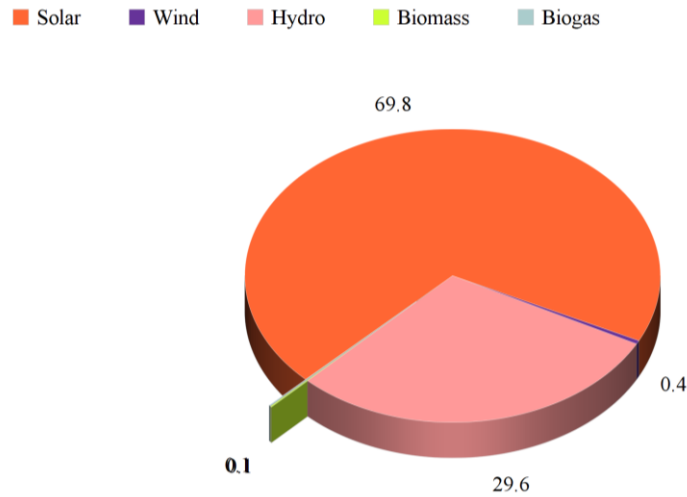
Figure 3: The contribution of different instigated renewable sources in Bangladesh [8]

Table 2: Advancement in the sector of renewable energy [9]

Methods	MW
Setups of Rooftop Photovoltaic at different offices	3.00
Solar PV Systems	150.00
Power generation by Hydro-electricity	230.00
Setups of Photovoltaics by the customers during new connections of Electricity	11.00
Setups of Photovoltaics on different shopping centres and commercial buildings	1.00
Solar Irrigation	1.00
Setups of Power Plants (Wind energy based)	2.00
Setups of Power Plants (Biogas- based)	5.00
Setups of Power Plants (Biomass-based)	1.00
Total	404.00

1.2 WIND ENERGY

The wind energy is a prominent and one of the most environmentally friendly energy sources available. Overview of a simplified wind power generation mechanism is represented in Figure 4. The kinetic energy of wind forces the turbine blade to rotate, which generates mechanical power for the turbine shaft. Finally, a generator is used to convert the mechanical power to electrical energy.

Theoretically, the power available in the wind can be estimated using the following equation-

$$P = \frac{1}{2} \times \rho \times A \times V^3 \qquad\qquad\qquad Eq\ (1.1)$$

Where, ρ= density of air (kg/m³), P= power generated (W), A = turbine blade swept area (m²), and V= Speed of wind (m/s). Although 59% power can be extracted theoretically (Betz Criterion) we can only produce 30-35% electricity.

While generating power from wind, the most important parameter that puts its effect is the speed of the wind. However, some other important factors also have their impact in wind power generation, which includes the number, size and orientation of the blades. These also play important impact on the efficiency of wind turbines. The wind turbines are classified based on the capacity of power generation into four main classes- large, medium, small and lastly micro scale wind turbines. Table 3 lists the main features of these different types of turbines. [10], [11]. Small-scale wind turbines are best for small-scale networks and domestic applications including charging and stand-alone power.
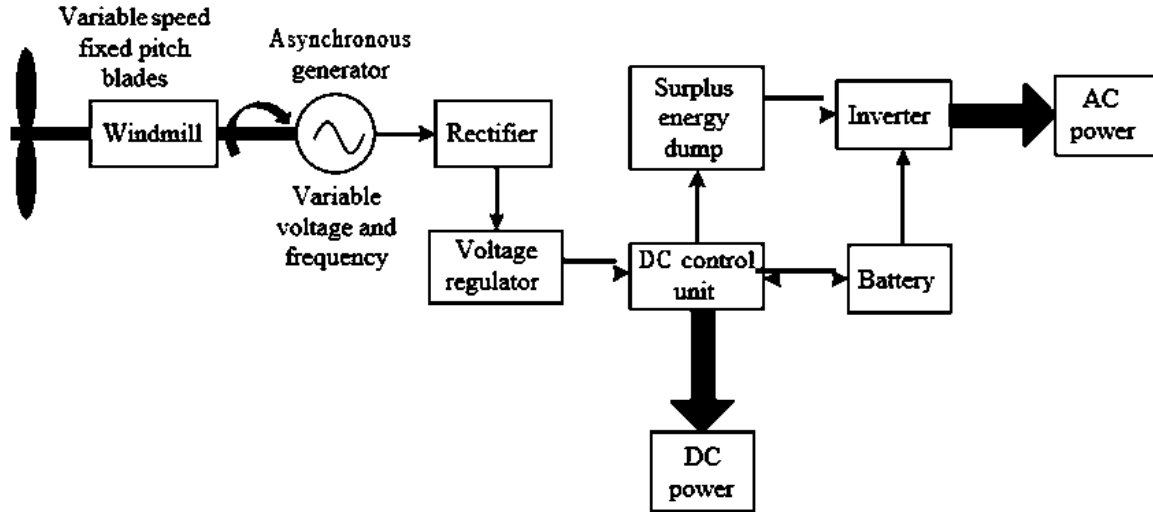
Figure 4: A simplified wind power generation mechanism overview [12]

Table 3: Taxonomy of wind turbine [10] [11]

Scale	Rotor diameter	Power Rating
Large	46 m and large	More than 1.0 MW
Medium	12 m to 45 m	40 kW to 999 kW
Small	3 m to 12 m	2 kW to 40 kW
Micro	Less than 3 m	50 W to 2 kW

Wind power generation has become very popular in last two decades as shown in Figure 5 [13]. It has increased by 35 GW and reached to 318 GW in 2013.

Wind power provided approximately 2.9% of world total electricity of the world in 2013. China is the largest to generate wind power among all the countries of the world. The total installed capacity of China in 2013 was 91.4 GW. From that 91.4 GW, 14.1 GW was used for connection of grid, and 75.5 GW was used for industrial operations. Among all the European countries, Germany produces the highest wing power. The installed capacity of Germany is 34.7 GW. Germany generated 53.4TWH of electricity of from wind energy. In South-Asia, India has 20.2 GW of installed capacity for wind turbine energy.

The figure shows gradual increase of wind power capacity from 2000 to 2013
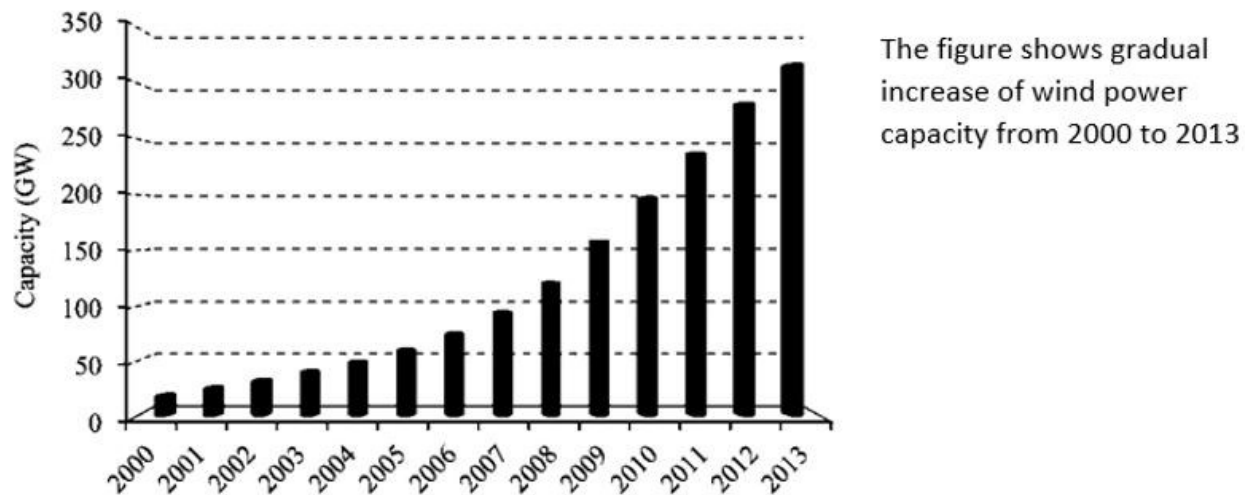
Figure 5: The total world capacity of wind power, year 2000–2013 [13]

Wind turbine can be a potential sources of energy for Bangladesh, because of its 724 km long coastline and several island in the Bay of Bengal, particularly during the rainy seasons. Normally, production of electricity at a large scale and while connected to the grid, a minimum of 7 m/s wind speed is required. However, 2.5 m/s wind speed can also generate power with upgraded blade design and aerodynamics. According to a study conducted by LGED, Bangladesh Metrological Department (BMD), and, Bangladesh center for advance studies (BCAS), wind speed in Bangladesh varies from 2.96 m/s to 4.54 m/s from 25m to 50m height [14]. For this reason, wind turbines at small scale are effective for some areas as depicted in Figure 6 in Bangladesh for stand-alone electricity [15].
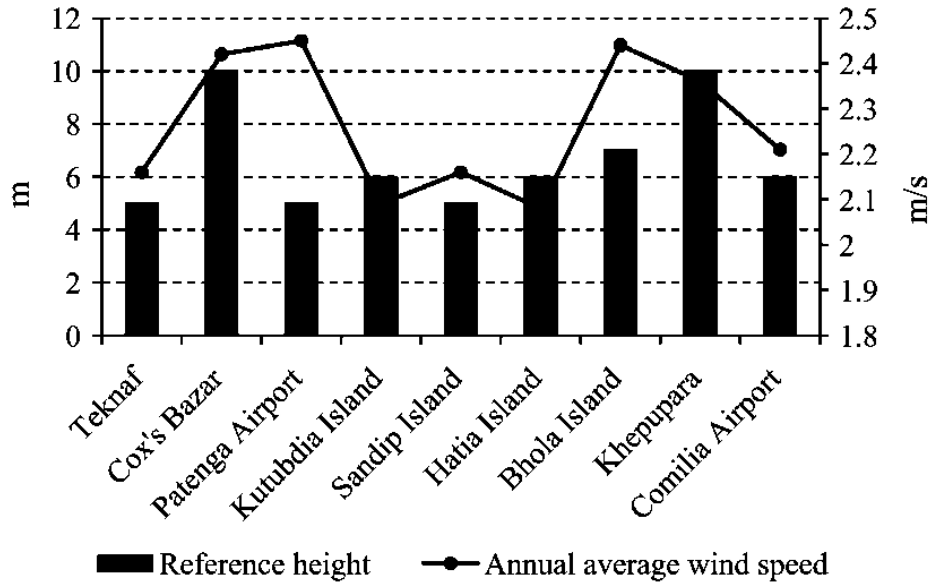
Figure 6: Wind speed of some sites in Bangladesh [15]

The first wind power generation plant installed in Bangladesh was 0.90 MW. BPDB installed in at Muduri dam in Feni. In 2008, BPDB constructed a new 1 MW wind battery power station on Kutubdia Island. The Kutubdia plant is comprised of fifty wind turbines, and each generates 20 KW. BPDB currently has 2 MW of installed wind power capacity [4]. Several governments as well as non-government institutions, in addition to BPDB, have constructed small-scale stand-alone and hybrid wind power facilities. A list of installed wind turbine by different organizations is as presented in Table 4.

Table 4: A scenario of wind turbine installations in Bangladesh [12]

Name of the organization	Installed Capacity (W)	Location	Type of application	Status
LGED	400	Kuakata	Wind-PV hybrid	Functioning
BRAC I	4320	Coastal region	Hybrid	Functioning
BRAC II	900	Coastal region	Stand-alone	Functioning
Grameen Shakti I	7500	Shelter for cyclone in the coastal region	Hybrid	Functioning
Grameen Shakti II	4500	The offices of Grameen in the coastal region	Hybrid	Functioning
Bangladesh Army	400	Chittagong hill tracts	Stand-alone	Functioning
IFRD I	600	Meghnaghat	Stand-alone	Functioning
IFRD II	1100	Teknaf	Stand-alone	Functioning

Bangladesh has recently performed several wind resources assessments at different places Bangladesh such as Mognamaghat of Cox's Bazar, Muhuri dam area of Feni, Parky beach of Anwara in Chittagong, Kuakata of Patuakhali and Kepupara of Borguna. Based on this assessment, BPDB has initiated another 15 MW capacity wind turbine power facility. A new pilot project with a wind power capacity of 0.90 MW at Kuakata is also planned. Moreover, Bangladesh also signed an agreement recently with the US DK Green energy (BD) Ltd. To install the largest wind power facility of the country at Cox's Bazar with a capacity of 60 MW which is a joint project of Denmark, Bangladesh and USA.

1.3 WIND TURBINE AND ITS TYPE

Horizontal-axis wind turbines (HAWTs) and vertical-axis wind turbines (VAWTs) are the two types of wind turbines in which they can be classified into.
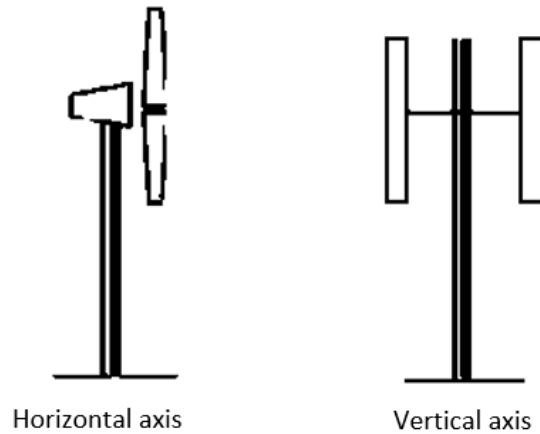
Figure 7: Types of wind turbine [16]

Initially, there was a perception that VAWTs are not economically suitable for large-scale electricity generation. For this reason, HAWTs have been in focus for the last few decades. However, there are several advantages of VAWTs over HAWTs. First, VAWT does not require complex yaw-mechanism. Secondly, VAWTs are omnidirectional and can generate electricity from wind from all directions. For these reasons, VAWTs offer energy solutions to remote locations which are disconnected from main distribution lines. Recently, mass production of VAWTs is started as small-scale wind turbines to provide electricity for remote locations.

1.4 A BRIEF OVERVIEW OF VAWT

VAWT has several advantages over other wind turbines. It was introduced by French engineer Darrieus first in 1931. However, it was not developed until the 1970s because of perception that, VAWT are not good for electricity generation. VAWTs are independent of wind direction, and have simplified yaw system. It is less expensive and requires lower maintenance cost. VAWTS are suitable and a cost-effective option for remote and rural environments. VAWT are classified into two major categories: lift-type (Darrieus) turbines and drag-type (Savonius). The Drag-type VAWT are normally not utilized for generation of electricity applications, because of it low efficiency.

Mainly, lift-type or Darrieus VAWT are used to generate small scale wind turbines. So, Darrieus VAWT is focused on in this study.

1.5 RESEARCH PROBLEM STATEMENT

Fossil fuel will run out within 50 years. Main energy sources will be solar, water and wind in future. Wind energy has a huge potential specially for remote locations and private use. However, horizontal axis wind turbines are very heavy because of its yaw mechanism.
VAWT does not require complex yaw mechanism and are omnidirectional. However, further research on mass production of VAWT and mechanism to increase its efficiency are required to provide electricity for remote locations.

1.6 GOALS AND OBJECTIVES OF THE STUDY

This work mainly concentrates on the simulation of a mini scale wind turbine for remote locations or private use. Simple endeavor of simulation that leads to further development of 2D and 3D simulations. The purpose of this study is rotor design optimization by studying the effects of various parameters like rotor radius, chord length etc.

1.7 SCOPE AND LIMITATION OF THE STUDY

In this project, the 2D simulation of a H-Darrieus VAWT was done using Computational Fluid Dynamics (CFD) simulation software Fluent. Sliding Mesh model was used which takes into account the vortices generated by the blades passing upwind on the blades downstream unlike over-simplified MRF model. This study can be used for design optimization for performance improvement of wind turbine. However, only simulation with validation is done with the intention of doing further studies on the performance evaluation of wind turbine. 2D simulations has its limitations as it doesn't consider 3D effects like tip vortex that leads to overestimation of generated power. So, the best results are expected to obtain by developing a 3D model. For running this type of transient simulations, a device with better capacity would be required.

1.8 METHODOLOGY OF THE STUDY

In this project first simulations were run for a H-Darrieus vertical axis wind turbine using a geometric domain that reflects the experimental scenario. Prior to running the final simulations, mesh independent and time independent studies were done to get an optimum mesh size and time step value. Simulations were run using the Sliding Mesh Model. As turbulence model, the transition SST model was used. From the simulations, an average moment coefficient was calculated that was used to ultimately calculate power coefficient at the corresponding tip speed ratio and a performance curve (C_p vs λ) was obtained. Finally, the result obtained from the simulations was validated with the experimental data.

1.9 MAIN FEATURES OF THE STUDY

The main features of the study are:

- The 2D simulation of a H-Darrieus VAWT was done using Computational Fluid Dynamics (CFD) simulation software Fluent.
- Cp vs λ curve obtained from the simulation matches considerably with the experimental data.
- Sliding Mesh model was used which takes into account the vortices generated by the blades passing upwind on the blades downstream unlike over-simplified MRF model.
- This study can be used for design optimization for performance improvement of wind turbine

1.10 ARRANGEMENT/ORGANIZATION OF THE THESIS

In chapter 1, an introduction to the of Bangladesh and the stance of wind energy are given. A brief overview of the wind energy, VAWT is presented. The need to focus on the research of wind turbine, problem statement, the scope, goals and objectives are discussed. A concise methodology along with the main features of the research are also mentioned in this introductory chapter.

In chapter 2, the state-of-the-art developments on wind turbine by the researchers is discussed. This chapter shows the gradual development in the research of VAWT and its design. Three approaches of the research are analytical, CFD and experimental. Of these three, at first analytical approach is discussed, followed by the CFD approach. And lastly, the combined approaches in the research are

discussed.

In chapter 3, the related theories about wind turbine and Computational fluid dynamics are discussed. This chapter begins with an introduction to the finite volume method. Then the theories related to the CFD are discussed where all the related governing equations are shown. Then the concepts related to wind turbine are discussed along with the appropriate equations.

In chapter 4, the simulation environment and the main methodology is provided. This begins with an introductory section of the fluid structure interaction. Then, the features of the experimental rotors are presented. Then all the simulation steps are discussed elaborately and sequentially, starting from the drawing of the geometry to the last step of running calculations in fluent. Lastly, the simulation fluid domain was summarized.

In Chapter 5, the simulation results and validation are presented. The first sections are the mesh and time independent studies. Then, the validation of the results is shown. Lastly, the velocity contour plot of the simulation is discussed.

Finally, in the chapter 6, at first, the whole work is summarized. In the second section, the significant concluding remarks are given. Lastly, some limitations and recommendations to address then are pointed and the possible future works are mentioned.

CHAPTER 2: LITERATURE REVIEW

The researches and industries are working on the rotor design optimization of VAWT to improve its performance. VAWT has some application-based advantages over the HAWT. Liu, Lin, and Zhang [17] have reviewed the commercial viability of VAWT. [18]. MacPhee and Beyene [18] focused on the Darrieus and Savonius rotors and worked on an extensive research on the latest works of the design of rotor and testing until the year 2012. Their work also reflects the advantage of VAWT in off grid and small scale applications. But for design optimization works, many parameters are there to consider, and experimentation is not always feasible. As a result, simulations are getting more importance and many researchers have worked on improving the simulation of VAWT. Ghasemian, Ashrafi, and Sedaghat [19] have reviewed the various CFD techniques of simulation for Darrieus VAWT.

However, it is very important to do some sort of validation before this simulation results can be trusted. Bedon et al. [20] have reviewed many databases of aerodynamic coefficients that are used for VAWT simulations. The comparison with the simulation results demonstrated considerable discrepancy so practical general considerations are recommended to the designers before deciding on the reliability of the simulations. So, careful validation remains a demanding step for simulation of VAWT.

Another approach is the analytical approach which can be very challenging, strenuous and extremely complicated. Mohammed et al. [21] have summarized and reviewed different momentum models. The momentum models include the double multiple streamtube (DMST) model, multiple streamtube model (MST) and single streamtube model (SST). Models other than momentum models include the vortex model and cascade model. [22]

The power coefficient of vertical axis wind turbines can be optimized using the tip speed ratio. [23]. Aslam Bhutta et al. [23] have reviewed the various design techniques and configurations of the vertical axis wind turbines. They studied different configurations of vertical axis wind turbines like the Darrieus rotors, Savonius rotors, combined Darrieus and Savonius rotors, Sistan wind mill, Zephyr tubine and observed how different power coefficients were obtained. They showed how power coefficient can be optimized using the tip speed ratio.

The current study focus on the 2D CFD simulation of a H-Darrieus vertical axis wind turbine where the turbulence SST model is chosen as the turbulence model. Validation of the simulation results are

also done with experimental result available in the literature.

2.1 ANALYTICAL STUDY APPROACH OF H-DARRIEUS VAWT

Starting from simple 1D equations Multiple Stream Tube Model or Vortex Method, researchers have continued their work to present day to capture the real characteristics of the complicated turbulence flow.

2.1.1 Momentum Model

2.1.1.1 Single Streamtube Model

Templin [24] proposed the single streamtube model and this model was used during the first attempt to study VAWT using momentum theory. This model can be used to estimate the lightly loaded wind turbine's overall performance. However, this overestimates the power than that of the experimental values. Variation of velocity of wind across the rotor is also not considered. [25]

2.1.1.2 Multiple Streamtube Model

This model is a more developed version of the Single Streamtube model developed by Wilson and P.B.S. [26] where the rotor is divided into a number of streamtubes. These streamtubes are independent and parallel. Then the blade element theories and the momentum theories are applied at each of these tubes. This model was then further developed by James H Strickland [27], Muraca, Stephens, and Dagenhart [28], Sharpe [29], Read and Sharpe [30]. Tai et al. [31] and Roh and Kang [32] have applied this model on H-Darrieus turbine and studied the performance.

2.1.1.3 Double-multiple Streamtube model

Paraschivoiu [33] has worked on the double-multiple stream tube (DMST) method for Darrieus type VAWT modelling. From their study, they have found that the double-multiple stream tube method includes dynamic stall and secondary effects that can be useful in structural design of Darrieus rotors.

Beri and Yao [34] have worked on the modelling of unsteady flow analysis of VAWT. Here also they used the double-multiple stream tube (DMST) method for the performance prediction of fixed pitched three blade VAWT with NACA 0018 blade profile. They also analyzed 2D unsteady flow with modified at the trailing edge using CFD. The comparing the power coefficient obtained from both DMST and CFD, it was observed that DMST showed negative torque generated at low tip

speed where CFD results showed positive torque. The maximum power coefficients of the two models also came at a normal range.

Paraschivoiu, Saeed, and Desobry [35] summarizes the progress made in the development of the different numerical tools for the simulation of the flow field around the VAWT as well as the dynamic-stall phenomenon of VAWT blades. The paper highlights the current capabilities and limitations of aerodynamic models with emphasis on double multiple stream tube (DMST) model as a design tool. This study concludes that further work is under consideration to develop improved models of the wind encountered by the rotor, the atmospheric flow across a site, the wake that affects blades in addition to the development of optimization tools.

2.1.2 Vortex Model

Strickland, Webster, and Nguyen [36] developed an aerodynamic prediction model for two-dimensional and three-dimensional Darrieus turbines where they have used vortex lattice method of analysis. A number of experiments were conducted in a water tow tank on several two dimensional setups of rotor. In general, there was a good match found between the experiments and analyses conducted. To analyze the near wake flow behind the rotors and to estimate instantaneous aerodynamic forces of blades, this model can be utilized. However, long computational time is required for the vortex model. As a results, instead of the long time consuming vortex models, most of the time the much simpler momentum model is used when only rotor power coefficient is required to be calculated. Often, additional work is required to be done in order to reach a periodic solution to reduce the high calculation time needed by the vortex model.

Wang, Zhang, and Zeng [37] validated a prospective flow 2-D vortex panel model of the straight blade vertical axis turbine with variable pitch for the calculation of unsteady hydrodynamics for the energy conversion of tidal streams. From this study, it was seen that the numerical results of predicted wake flow of the rotor and instantaneous blade forces showed a good accordance with that of the test data. The previous standard free vortex model as well as vortex method combined with finite element analysis was also compared which showed that the 2D vortex panel model was far better than that of the previous mode yet less complicated than that of the latter one and appropriate for optimization as well as designing of the VAWT with straight blades.

2.1.3 Cascade Models

Hirsch and Mandal [38] first applied the cascade model to VAWT. This model is not seeming to be applied widely in the literature. Overall, the performance of this model is satisfactory and unlike the streamtube model, it does not have any problem with convergence. Hand and Cashman [39] and Hand, Cashman, and Kelly [40] have applied this model to study H-Darrieus VAWT.

However, these models are first attempt designs and they need to be validated. Wind tunnel experiments are need to be conducted for their validation which is expensive considering both time and cost. So, another approach to study their aerodynamic behavior is to study using CFD.

2.2 COMPUTATIONAL FLUID DYNAMICS SIMULATION

2.2.1 Considering Different Turbulence Models

Many turbulence models are developed and still are studied for improvements to capture the complex and unruly behaviour of the turbulence.

Rezaeiha, Montazeri, and Blocken [41] compared commonly used seven turbulence models of eddy-viscosity for the simulations of VAWT in CFD. The models include one to four equations, viz. the realizable k-ε, Spalart-Allmaras, RNG k-ε, SST k-ω, SST k-ω with an additional intermittency transition model (SSTI), transition SST (TSST) k-ω models and k-kl-ω models. Besides, the comparison includes the inviscid modeling. The blade aerodynamics, turbine power performance, and turbine wake, are all being studied. Incompressible unstable URANS simulations with high fidelity were used. By analysis, it is seen that the simulation results are highly sensitive to the turbulence model which is particularly true for the CP turbine power coefficient. The k-kl-ω models, SA inviscid, RNG k-ε, and realizable k-ε all fail to reproduce the aerodynamic performance of VAWT, according to the findings. Only SST type models (TSST, SSTI, and SST k-ω) demonstrate rational compromise with all experimental data, with the transitional SST k-ω types (SSTI and TSST) recommended, particularly in the transitional flow regime.

In this study, the transition SST model was used for 2D simulation of H-Darrieus VAWT.

2.2.1.1 k-ε model

Daróczy et al. [42] have studied different turbulence models for the simulation of H-Darrieus turbine. By comparing with experimental results, it was found that the k-ε and k-ω SST model

showed better results for 2D simulation.

Howell et al. [43] applied the k-ε for both 2D and 3D simulations and it was observed that, while better results were obtained in 3D simulation, the k-ε model overestimated the performance coefficient in 2D simulation.

Untaroiu et al. [44] employed the standard k-ε model to study the self-starting behaviour of H-Darrieus turbine in both 2D and 3D simulations where both failed to estimate the behaviour, especially the 3D simulation. So, it was recommended not to use this model to estimate the self-starting behaviour of VAWT, and mainly not for 3D simulations.

2.2.1.2 k-ω (SST) model

This model is a combination of two models- the k-ε and k-ω turbulence models. [38].

McNaughton, Billard, and Revell [45] made a comparison among the different turbulence models to estimate the structure of turbulent flow. They observed that at low Reynolds number, correctly prediction can be done regarding the leading-edge vortex formations.

Edwards, Angelo Danao, and Howell [46] studied the blade lift coefficient using different models and this model yielded the best result.

Almohammadi et al. [47] studied the dynamic stall behavior of blade using two different models and observed that stalling occurs later for this model than that of the transition SST model.

2.2.1.3 Transition SST model

Arab et al. [48] have studied the self-starting characteristics of turbine and observed that the aerodynamic performance of the turbine could be influenced by the flow-field history. It was also observed that the inertia of the rotor can put an effect on the self-starting characteristics of the turbines.

Balduzzi et al. [49] studied the 3D flow effects using this model. It was observed that the 3D flow effects put their impact the blade torque by 8.6% which affect the energy efficiency.

Lam and Peng [50] have focused on the wake characteristics of the turbine on both 2D and 3D models. It was observed that the 2D models could not estimate the characteristics satisfactorily.

In general, the fully turbulent RANS model shows a tendency to overestimate the power due to strenuous stall phenomena predictions. Hence, transition SST model was used in this study with the intention to obtain better results.

2.3 COMBINED STUDIES (ANALYTICAL, CFD AND EXPERIMENTAL)

Raciti Castelli, Englaro, and Benini [51] developed a computational fluid dynamics model for the investigation of aerodynamic forces on a straight blade Darrieus vertical-axis wind turbine, as well as energy performance evaluation. In this attempt, the significant principles of BEM theory that does estimation of performance of rotor are transferred to the CFD codes that allow the correlation of the dynamic quantities like torque of the rotor, tangential and normal forces of blade with flow geometry properties like angle of attack of blades. This model can be addressed as a very powerful design and optimization tool for developing new architectures of rotor when experimental data are available. In this paper, the simulation for a three bladed classical NACA 0021 rotor is suggested after evaluating the computational model against experimental data. The flow characteristics are studied for a number of different tip speed ratios. This allows better understanding of basic physics of the vertical axis wind turbine as well as comparison of rotor working at optimum and lower Cp values. From this study, the average rotor power coefficient was found to be lower. However, three times every rotor revolution, the instantaneous power coefficient surpasses the Betz's limit the reason which need to be investigated further as it defies the well-established theory.

With an emphasis on the stream tube technique, Biadgo et al. [52] examines the progress made in the advancement of aerodynamic models for Vertical-Axis Wind Turbines studies. In order to evaluate the performance of a fixed pitch straight blade NACA 0012 airfoil profiled vertical axis wind turbine, both analytical and numerical studies were carried out. ANSYS FLUENT was employed to simulate 2D and unsteady flow around the same model that solved the RANS equations. Lastly, the CFD simulation findings were compared with the analytical calculations of the DMST i.e. the double multiple stream tube model. The Cp values of both the models were compared and it was observed that the DMST model overestimated the maximum Cp value. The modeled turbine's DMST and CFD results showed minimum and/or negative torque showing that NACA0012 is unable to self-start.

Sabaeifard, Razzaghi, and Forouzandeh [53] investigates the impact of different parameters of design like the type of airfoil, the solidity of the turbine, the number of blades on the straight blade Darrieus type small scale VAWT's performance. For transient simulations, the K-ε turbulence model is used. And to express the dimensionless form of power output of the wind turbine as a function of wind velocity (free stream velocity) and rotational speed of the rotor, the MRF model

i.e. the multiple reference frame model capability of CFD solver is used. The improved turbine had a highest power coefficient of 0.36 and 0.32 in CFD calculations and wind tunnel testing, respectively, with a tip speed ratio of 3.5.

Gupta and Biswas [54] used FLUENT 6.2 software to undertake a steady-state and 2D CFD investigation on the efficiency of a twisted three-bladed H-Darrieus rotor. To solve momentum and mass conservation equations, the flow across the rotor was modeled using an unstructured-mesh FVM combined with a moving mesh methodology. The turbulence model k-ε was used as the basis. For pressure-velocity coupling, a second-order upwind discretization approach was used. For two chord Reynolds numbers, aerodynamic coefficients like drag coefficients, lift coefficients as well as the lift-to-drag coefficients were analyzed with regard to the AoA. The rotor's power coefficient was assessed. To verify the findings, the experimental values were used. The tests were previously carried out in a subsonic wind tunnel and results demonstrated that the two approaches were very similar.

Simão Ferreira et al. [55] compared the findings of URANS (k-ε and Spalart Allmaras) with large eddy models (Detached Eddy Simulation and Large Eddy Simulation). The results of the Detached Eddy Simulation turbulence model were the most similar to those of the experiments. Moreover, the DES model not only predicts the shedding and creation of vorticity and the convection of vorticity, but also has a low sensitivity to the refinement of mesh (both in space and time), which makes it appropriate for simulation with limited or no validation data. The difficulty of URANS models to appropriately model huge eddies rendered them ineffective. The LES model behaved poorer than that of the DES model, most likely as a result of inaccurate wall modeling.

CHAPTER 3: THEORY

3.1 FINITE VOLUME METHOD- AN OVERVIEW

In resolving the partial differential equations, the Finite Volume Method is one of the most powerful and widely used numerical methods. It is a numerical method where the PDE expressing conservation laws over the differential volumes are transformed into distinct algebraic equations over finite volumes (or elements or cells). Just like the finite difference method or finite element method, discretization of the geometric domain is the first step of this method also. Discretization into non-overlapping elements or finite volumes of the entire geometric domain into algebraic equations is done. The PDE are then transformed or discretized into algebraic equations and this is done by integrating them over all the distinct elements. Next, the values of the dependent variables at each of the elements are calculated by solving the system of algebraic equations.

In this method, sometimes, some of the terms turns into face fluxes in the conservation equation and are evaluated in the faces of the finite volumes. Here, the flux entering a particular volume is equal to that of the flux leaving the adjacent volume. Hence, this method is conservative. So this method is mostly preferred in CFD due to this inherent conservation property. This method also has other important features. This can be applied to solve complex geometries as it can be formulated in the physical space on unstructured polygonal meshes. It also provides another advantage- since the unknown values are calculated at the cell centers or centroids of the volume elements, FVM can be implement a variety of boundary conditions.

All these advantages and characteristics have made the FVM one of the most applicable numerical techniques to solve numerical simulations of a wide variety of applications including heat and mass transfer, fluid flow etc. This method's improvement is closely entwined with CFD, and now is applied to solve complex geometries and applications. [56]
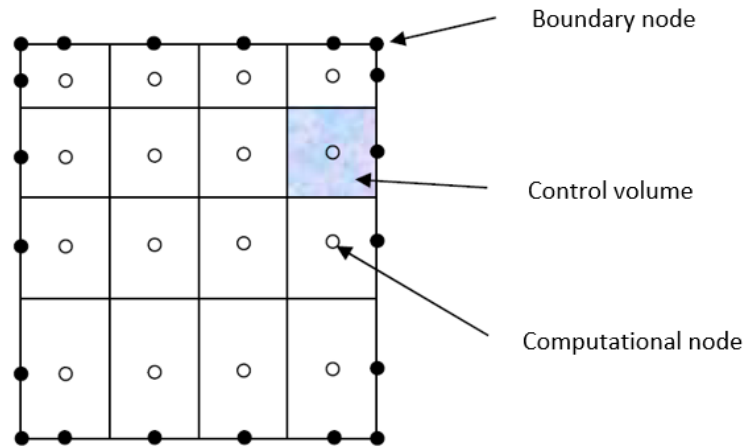
Figure 8: Finite Volume Method grid [57]

3.2 COMPUTATIONAL FLUID DYNAMICS (CFD)

The Computational Fluid Dynamics is a branch of fluid dynamics that offers an economical way to simulate actual flows by the numerical solution of the governing equations (GE) [58]. CFD has its non-industrial and industrial applications for their less cost and time demands in model design works [59]. We require mathematical equations that best represent fluid motion in order to assess a fluid problem using CFD.

3.2.1 Governing Equation

The Fluid dynamics problems are all based on three fundamental physical principles:

- Mass conservation
- Momentum equation
- Energy conservation

3.2.1.1 Mass Conservation

The principle of mass conservation states that the rate of mass flow into a fluid element (volume) equals the rate of mass increase in the fluid element (volume) [59], so, for a compressible fluid, we can write:

$$\frac{\partial \rho}{\partial t} + \text{div}(\rho \mathbf{u}) = 0 \qquad \qquad \textbf{\textit{Eq (3.1)}}$$

where ρ is fluid density and $\boldsymbol{u}$ is the velocity vector in Cartesian coordinates

An incompressible fluid, such as liquid, has a constant density ($\frac{\partial \rho}{\partial t} = 0$); so,

$$div \, \boldsymbol{u} = 0 \qquad \qquad \textbf{\textit{Eq (3.2)}}$$

21

or,

$$\frac{\partial u}{\partial x} + \frac{\partial v}{\partial y} + \frac{\partial w}{\partial z} = 0 \qquad \qquad Eq\ (3.3)$$

where velocity components of $\boldsymbol{u}$ are u, v, and w.

3.2.1.2 Momentum equation

Newton's second law states that the sum of forces acting on fluid particles equals the rate of change of momentum. Surface forces can be separated into independent terms and body forces can be separated as source term. [59]. The momentum equations in three directions can then be obtained by expressing the stresses as pressures on a control volume. As a result, the x, y, and z components of the momentum equation equal:

$$\frac{\partial(\rho u)}{\partial t} + \text{div}(\rho u\mathbf{u}) = \frac{\partial(-p + \zeta_{xx})}{\partial x} + \frac{\partial \zeta_{yx}}{\partial y} + \frac{\partial \zeta_{zx}}{\partial z} + S_{Mx} \qquad Eq\ (3.4)$$

$$\frac{\partial(\rho v)}{\partial t} + \text{div}(\rho v\mathbf{u}) = \frac{\partial \zeta_{xy}}{\partial x} + \frac{\partial(-p + \zeta_{yy})}{\partial y} + \frac{\partial \zeta_{zy}}{\partial z} + S_{My} \qquad Eq\ (3.5)$$

$$\frac{\partial(\rho w)}{\partial t} + \text{div}(\rho w\mathbf{u}) = \frac{\partial \zeta_{xz}}{\partial x} + \frac{\partial \zeta_{yz}}{\partial y} + \frac{\partial(-p + \zeta_{zz})}{\partial z} + S_{Mz} \qquad Eq\ (3.6)$$

Where, S_{Mx}, S_{My} and S_{Mz} are body forces (source term), for example the value of body forces due to the gravity will be are body forces (source term), [59]: $S_{Mx} = 0$, $S_{My} = 0$ and $S_{Mz} = -\rho g$. Navier-Stokes equations are used to calculate the stress components

3.2.1.3 Energy Conservation

The energy equation is derived from the first law of thermodynamics, which states that fluid particle's rate of energy change equals the addition of heat addition rate and the work done rate on the particle. [59]. Thus, the energy equation can be written:

$$\frac{\partial(\rho i)}{\partial t} + \text{div}(\rho i\mathbf{u})$$

$$= -p \ \text{div}\ \mathbf{u} + \text{div}\ (\boldsymbol{k}\ grad\ \boldsymbol{T}) + \zeta_{xx}\frac{\partial u}{\partial x} + \zeta_{yx}\frac{\partial u}{\partial y} + \zeta_{zx}\frac{\partial u}{\partial z} \qquad Eq\ (3.7)$$

$$+ \zeta_{xy}\frac{\partial v}{\partial x} + \zeta_{yy}\frac{\partial v}{\partial y} + \zeta_{zy}\frac{\partial v}{\partial z} + \zeta_{xz}\frac{\partial w}{\partial x} + \zeta_{yz}\frac{\partial w}{\partial y} + \zeta_{zz}\frac{\partial w}{\partial z}$$

$$+ S_i$$

where $\boldsymbol{T}$ is the temperature, i is the internal energy, $\boldsymbol{k}$ is the thermal conductivity, u, v and w are the velocity components of $\mathbf{u}$, p is the pressure, and S_i is a new source term $S_i = S_E - \boldsymbol{u}\ S_{\boldsymbol{k}}$ which S_E is a energy source and $S_{\boldsymbol{k}}$ is a source of Mechanical (Kinetic) energy.

Hence, the energy equation for compressible fluids can be written as:

$$\frac{\partial(\rho h_o)}{\partial t} + div(\rho h_o \boldsymbol{u})$$

$$= div(\boldsymbol{k}\,grad\,\boldsymbol{T}) + \frac{\partial \rho}{\partial t} + \frac{\partial(u\zeta_{xx})}{\partial x} + \frac{\partial(u\zeta_{yx})}{\partial y} + \frac{\partial(u\zeta_{zx})}{\partial z}$$

$$+ \frac{\partial(v\zeta_{xy})}{\partial x} + \frac{\partial(v\zeta_{yy})}{\partial y} + \frac{\partial(v\zeta_{zy})}{\partial z} + \frac{\partial(w\zeta_{xz})}{\partial x}$$

$$+ \frac{\partial(w\zeta_{yz})}{\partial y}\frac{\partial(w\zeta_{zz})}{\partial z} + S_h$$

Eq (3.8)

where S_h is a source of enthalpy energy, and h_0 is the specific total enthalpy.

3.2.1.4 Navier-Stokes Equations

In the previous equations, the viscous stress components($Ç_{ij}$) are some unknown variables. For most fluid flows, these values could be achieved by supplying the appropriate model, that is expressed as functions of the local rate of deformation. In three-dimensional flows, the local rate of deformation is composed of the linear and volumetric deformation rates. [59]. In case of compressible flows, Newton's law of viscosity is made up of two constant viscosities: dynamic viscosity, which is connected to linear deformations, and volumetric viscosity, which is associated with volumetric deformations. As a result, three of the six viscous stress components are constant and six are changeable. These elements are described as follows:

$$\zeta_{xx} = 2\mu \frac{\partial u}{\partial x} + \lambda\,div\,\boldsymbol{u} \qquad\qquad \text{Eq (3.9)}$$

$$\zeta_{yy} = 2\mu \frac{\partial v}{\partial y} + \lambda\,div\,\boldsymbol{u} \qquad\qquad \text{Eq (3.10)}$$

$$\zeta_{zz} = 2\mu \frac{\partial w}{\partial z} + \lambda\,div\,\boldsymbol{u} \qquad\qquad \text{Eq (3.11)}$$

$$\zeta_{xy} = \zeta_{yx} = \mu \left(\frac{\partial u}{\partial y} + \frac{\partial v}{\partial x}\right), \qquad\qquad \text{Eq (3.12)}$$

$$\zeta_{xz} = \zeta_{zx} = \mu \left(\frac{\partial u}{\partial z} + \frac{\partial w}{\partial x}\right), \qquad\qquad \text{Eq (3.13)}$$

$$\zeta_{yz} = \zeta_{zy} = \mu \left(\frac{\partial v}{\partial z} + \frac{\partial w}{\partial y}\right). \qquad\qquad \text{Eq (3.14)}$$

By substituting the equations 3.12 to 3.14 to equations 3.4 to 3.6 we will reach to the Navier-Stokes equations:

$$\frac{\partial(\rho u)}{\partial t} + div(\rho u\boldsymbol{u}) = -\frac{\partial p}{\partial x} + div\,(\mu\,grad\,u) + S_{Mx} \qquad\qquad \text{Eq (3.15)}$$

$$\frac{\partial(\rho v)}{\partial t} + \text{div}(\rho v\mathbf{u}) = -\frac{\partial p}{\partial y} + div\ (\mu\ grad\ v) + S_{My} \qquad \textbf{\textit{Eq (3.16)}}$$

$$\frac{\partial(\rho w)}{\partial t} + \text{div}(\rho w\mathbf{u}) = -\frac{\partial p}{\partial z} + div\ (\mu\ grad\ w) + S_{Mz} \qquad \textbf{\textit{Eq (3.17)}}$$

3.2.2 Finite Volume Method

One of the most popular discretization method used in CFD is the Finite Control Volume Method which is commonly known as the Finite Volume Method. In this method, first the main
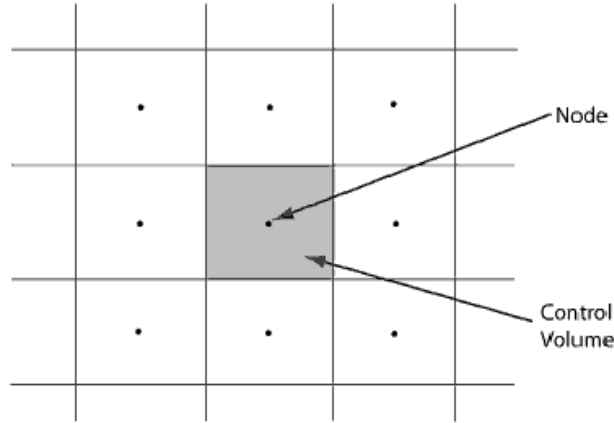
Figure 9: A typical 2D finite volume grid (rectangular grid) [88]

domain is discretized into finite control volumes and then over each of the control volumes, integration is done. The finite volume method has some similarity with finite difference and finite element methods where the discretization part is very similar to that of the finite element method. However, finite volume method's computational effort is higher than that of finite difference method but less than that of the finite element method when accuracy is almost similar. Besides, the FVM offers some advantages over the other two methods. FVM is based on cell average value. This is why, it provides some advantages like conservation of momentum, mass and energy is maintained at local scales. In addition, this can enable to work with geometry with complex shapes. [60]

The general conservation equation is equal to:

$$\frac{\partial(\rho\varphi)}{\partial t} + \text{div}(\rho\varphi\mathbf{u}) = \text{div}(\Gamma\ grad\ \varphi) + S_\varphi \qquad \textbf{\textit{Eq (3.18)}}$$

where φ is a fluid property and Γ is the diffusion coefficient.

By integration of equation 3.18 over a control volume, the equation becomes:

$$\int_{CV} \frac{\partial(\rho\varphi)}{\partial t}dV + \int_{CV} div(\rho\varphi\mathbf{u})dV = \int_{CV} div(\Gamma\ grad\ \varphi)dv + \int_{CV} S_\varphi dv \qquad \textbf{\textit{Eq (3.19)}}$$

24

By applying Gauss' divergence theorem, equation 3.19 can be written as follows:

$$\frac{\partial}{\partial t}\left(\int_{CV} \rho\varphi dv\right) + \int_A \boldsymbol{n} \cdot (\rho\varphi\mathbf{u})dA = \int_A \boldsymbol{n} \cdot (\Gamma \operatorname{grad} \varphi)dA + \int_{CV} S_\varphi dv \qquad \textit{Eq (3.20)}$$

The change rating term of 3.19 for the steady state problems is equal to zero, therefore,

$$\int_A \boldsymbol{n} \cdot (\rho\varphi\mathbf{u})dA = \int_A \boldsymbol{n} \cdot (\Gamma \operatorname{grad} \varphi)dA + \int_{CV} S_\varphi dv \qquad \textit{Eq (3.21)}$$

And for the transient problems, the equation will be:

$$\int_{\Delta t} \frac{\partial}{\partial x}\left(\int_{CV} (\rho\varphi)dv\right) dt + \int_{\Delta t}\int_A \boldsymbol{n} \cdot (\rho\varphi\mathbf{u})dA\, dt$$
$$= \int_{\Delta t}\int_A \boldsymbol{n} \cdot (\Gamma_\varphi \operatorname{grad} \varphi)dA\, dt + \int_{\Delta t} S_\varphi dvdt \qquad \textit{Eq (3.22)}$$

3.2.3 Turbulence Modelling

The turbulence flow is a highly erratic flow of fluid (gas or liquid) where the various properties like velocity continuously fluctuates in different directions. The equations to describe such kind of flow is very complex, and they are nonlinear, and time-dependent. It is very complicated to use the Navier-Stokes equations for these flows where the equations are three dimensional. As a result, for calculating industrial flows, most commonly, the Reynolds Averaged Navier-Stokes Equation (RANS) is used. The RANS equations are obtained by taking the mean of different properties like mean pressure, mean velocities, mean stresses etc. and plugging them into the Navier-stokes equations. Hence, the equations 3.15 to 3.17 become

$$\frac{\partial(\rho U)}{\partial t} + \operatorname{div}(\rho U\mathbf{U})$$
$$= -\frac{\partial P}{\partial x} + \operatorname{div}(\mu \operatorname{grad} U) \qquad \textit{Eq (3.23)}$$
$$+ \left[-\frac{\partial(\rho \overline{u'^2})}{\partial x} - \frac{\partial(\rho \overline{u'v'})}{\partial y} - \frac{\partial(\rho \overline{u'w'})}{\partial z}\right] + S_{Mx}$$

$$\frac{\partial(\rho V)}{\partial t} + \text{div}(\rho V \mathbf{U})$$

$$= -\frac{\partial P}{\partial y} + div\,(\mu\; grad\; V) \qquad\qquad \textit{Eq (3.24)}$$

$$+ \left[-\frac{\partial(\rho \overline{u'v'})}{\partial x} - \frac{\partial(\rho \overline{v'^2})}{\partial y} - \frac{\partial(\rho \overline{v'w'})}{\partial z} \right] + S_{My}$$

$$\frac{\partial(\rho W)}{\partial t} + \text{div}(\rho W \mathbf{U})$$

$$= -\frac{\partial P}{\partial z} + div\,(\mu\; grad\; W) \qquad\qquad \textit{Eq (3.25)}$$

$$+ \left[-\frac{\partial(\rho \overline{u'w'})}{\partial x} - \frac{\partial(\rho \overline{v'w'})}{\partial y} - \frac{\partial(\rho \overline{w'^2})}{\partial z} \right] + S_{Mz}$$

The turbulent stresses, also known as Reynolds stresses, are added to the equation on the mean velocity components U, V, and W.

where:

$$\boldsymbol{U = u - u'};\; U = u - u';\; V = v - v';\; W = w - w';\; P = p - p'$$

U, V, W are the mean velocity components of U; u′, v′, w′ are the fluctuation velocity components of u′; and e′ is the mean and fluctuating component of pressure.

The Reynolds stresses can be calculated using mean deformation rates, which are equal to:

$$\tau_{ij} = -\rho \overline{u_i' u_j'} = \mu_t \left(\frac{\partial U_i}{\partial x_j} + \frac{\partial U_j}{\partial x_i} \right) \qquad\qquad \textit{Eq (3.26)}$$

where μ_t is the turbulent viscosity which can be calculated using many methods.

3.2.3.1 The K-ε Model

The k-ε model is considered for free stream fluid. For turbulent kinetic energy, k, this model has one equation and this model has another equation for the turbulent dissipation rate, ε. Therefore, by using the equation below, the turbulence viscosity for the k-ε model can be obtained:

$$\mu_t = \rho C_\mu \frac{\kappa^2}{\varepsilon} \qquad\qquad \textit{Eq (3.27)}$$

where C_μ is a dimensionless constant. By using the following equations, k and s can be obtained:

$$\frac{\partial(\rho \kappa)}{\partial t} + \text{div}(\rho \kappa \mathbf{U}) = div \left[\left(\mu + \frac{\mu_t}{\sigma_\kappa} \right) grad\; \kappa \right] + P_\kappa - \rho \varepsilon \qquad\qquad \textit{Eq (3.28)}$$

$$\frac{\partial(\rho \varepsilon)}{\partial t} + \text{div}(\rho \varepsilon \mathbf{U}) = div \left[\left(\mu + \frac{\mu_t}{\sigma_\varepsilon} \right) grad\; \varepsilon \right] + \frac{\varepsilon}{\kappa} - (C_{\varepsilon 1} P_\kappa - C_{\varepsilon 2} \rho \varepsilon) \qquad\qquad \textit{Eq (3.29)}$$

P_κ is the turbulence production and $\sigma_\kappa, \sigma_\varepsilon, C_{\varepsilon 1}$ and $C_{\varepsilon 2}$ are constants and equal to:

$$\sigma_\kappa = 1 \;;\; \sigma_\varepsilon = 1.3 \;;\; C_{\varepsilon 1} = 1.44 \;;\; C_{\varepsilon 2} = 1.92$$

3.2.3.2 The K-ω Model

For calculating turbulence near the wall, the k-ω model is the most appropriate model. For the specific dissipation rate, ω and for the turbulence kinetic energy, k, this model takes the basis of model transport equations. Using the equations below, the values are obtained:

$$\frac{\partial(\rho\kappa)}{\partial t} + \text{div}(\rho\kappa\mathbf{U}) = div\left[\left(\mu + \frac{\mu_t}{\sigma_\kappa}\right) grad\ \kappa\right] + P_\kappa - \beta'\rho\kappa\omega \qquad \textit{Eq (3.30)}$$

$$\frac{\partial(\rho\boldsymbol{\omega})}{\partial t} + \text{div}(\rho\boldsymbol{\omega}\mathbf{U}) = div\left[\left(\mu + \frac{\mu_t}{\sigma_\omega}\right) grad\ \omega\right] + \alpha\frac{\omega}{\kappa}P_\kappa - \beta\rho\omega^2 \qquad \textit{Eq (3.31)}$$

$\sigma_\kappa, \sigma_\varepsilon, \alpha, \beta, and\ \beta'$ are constants and equal to:

$$\sigma_\kappa = 1;\ \ \sigma_\varepsilon = 2;\ \ \alpha = \frac{5}{9};\ \ \beta = 0.075;\ \ \beta' = 0.09$$

Therefore, the turbulence viscosity of this model will be:

$$\mu_t = \rho\frac{k}{\omega} \qquad \textit{Eq (3.32)}$$

There are some advantages of using the k-ω model. Near the wall, this model uses low Reynolds number. This enables easier modelling, and as a result the result obtained becomes more accurate and also more robust. However, this model also has some disadvantages. This model is very much sensitive to the free stream conditions.

3.2.3.3 The Shear-Stress Transport (SST) Model

The SST model is a combination of both the k-ω model and the k-ε model. This model combines the best effects of both the models. Near the wall region, it makes the use of the k-ω model which gives better results at near the wall region. On the other hand, in free-stream flow regions, it makes the use of k-ε model. Thus it combines the best effects of both the models and implements to obtain the best result. However, it is mainly based on the k-ω model and has the similar wall treatment capability automatically.

3.3 WIND TURBINE TERMS

3.3.1 Tip Speed Ratio

In wind turbine design, the TSR i.e. the Tip Speed Ratio is one of the most important factors to consider. It is the ratio between the wind turbine blades' tips' speed to the speed of the wind. The tip speed ratio depends on a number of factors like the number of turbine blades, the wind turbine type and the airfoil profile of the blade.

$$TSR = \frac{\omega r}{v}$$

Eq (3.33)

where,

ω= rotational speed of turbine in rad/sec

r= rotor radius

v=speed of relative wind

3.3.2 Power Co-Efficient and Its Calculation

The power coefficient (C_p) is an important term that is very commonly used for wind turbine performance evaluation. It is the fraction of power available in the wind that is produced as electrical output [61]. (Depends on wind and rotor speed)

$$C_p = \frac{P_t}{P_a} = \frac{M\omega}{\frac{1}{2}\rho A v^3}$$

Eq (3.34)

The total moment M is calculated in Fluent using the moment coefficient Cm, which is specified as:

$$C_m = \frac{M}{\frac{1}{2}\rho A v^2 L}$$

Eq (3.35)

C_p can be calculated from C_m:

$$C_p = \frac{C_m \frac{1}{2}\rho v^2 A L \omega}{\frac{1}{2}\rho A v^3} = C_m \frac{\omega L}{v}$$

Eq (3.36)

In 2D simulations, the value of A corresponds to the diameter of the turbine, while the value of L corresponds to the radius of the turbine. [62]. Applying these changes to the equation:

$$C_p = C_m \frac{\omega R}{v}$$

Eq (3.37)

Using the definition of the tip speed ratio (TSR):

$$C_p = C_m \lambda$$

Eq (3.38)

3.3 C_p Vs λ Curve

The C_p vs λ curves are most commonly drawn in the wind turbine industry for performance evaluation. C_p vs curves is used in wind turbine design to calculate rotor output for every wind and rotor speed combination.

These curves give us fast feedback on the highest rotor power coefficient and the best tip speed ratio.

After a rotor is designed, it does its optimum operation at a particular tip speed ratio. After designing, it is required to be acknowledged about the rotor's performance over all possible TSR. It is required to determine the aerodynamic conditions at each of the section of the blades for each TS and from this it is possible to evaluate the total rotor performance. This result is commonly expressed in a graphical format and this graph is the C_p vs λ curve.

The shape of the curve is bell shaped as shown in the figure 10. When tip speed ratio is zero, the rotor remains stationary and do not harness any wind power. On the other hand, when the TSR is very high, the rotor runs very fast and it appears like a complete blocked disc to the wind. The wind then flows around this blocked disc so that there is not transport of mass through the rotor. This creates a situation that do not enable any power extraction from the wind.

Between these zero TSR and very high TSR, there is an optimum TSR value at which the turbine can extract the maximum power. This maximum power is limited by Betz law. At this optimum TSR condition, the velocity of the rotor disc is two-third of the speed of the wind according to the Betz law. [63]

Figure 10: A typical C_p vs λ curve [64]
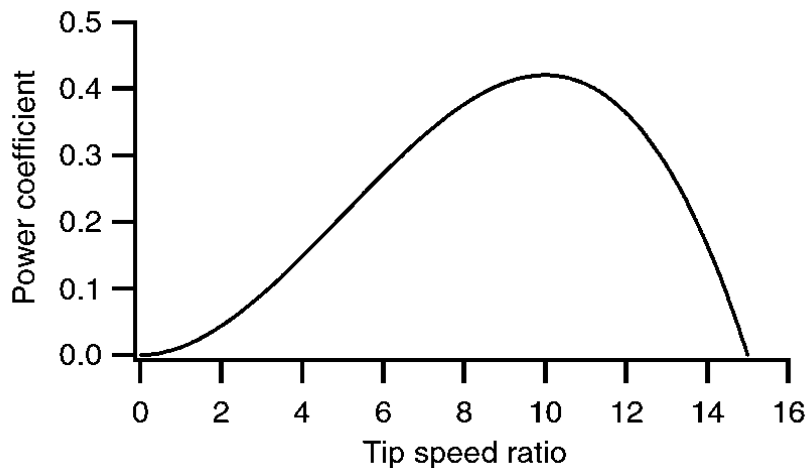
The first or the most important task here was to get the C_p vs. λ curve for this study. In order to obtain the C_p vs. λ curve, the moment coefficient value had to be obtained for each value of λ.

So, before getting into the plot, more about the characteristics of moment coefficient should be known first and so, more details are clarified here. For this type of problem, a periodic pattern is observed for the moment coefficient. The fluent lets us to get an instantaneous value of this parameter not only for the airfoils individually or for the entire turbine as a whole. The ultimate cyclical moment coefficient is then obtained by summing as the instantaneous values. It works in a sinusoidal manner, and so, the mean value is calculated in order to get to the actual or real value.

Figure 11 depicts a moment coefficient plot obtained from a typical simulation:
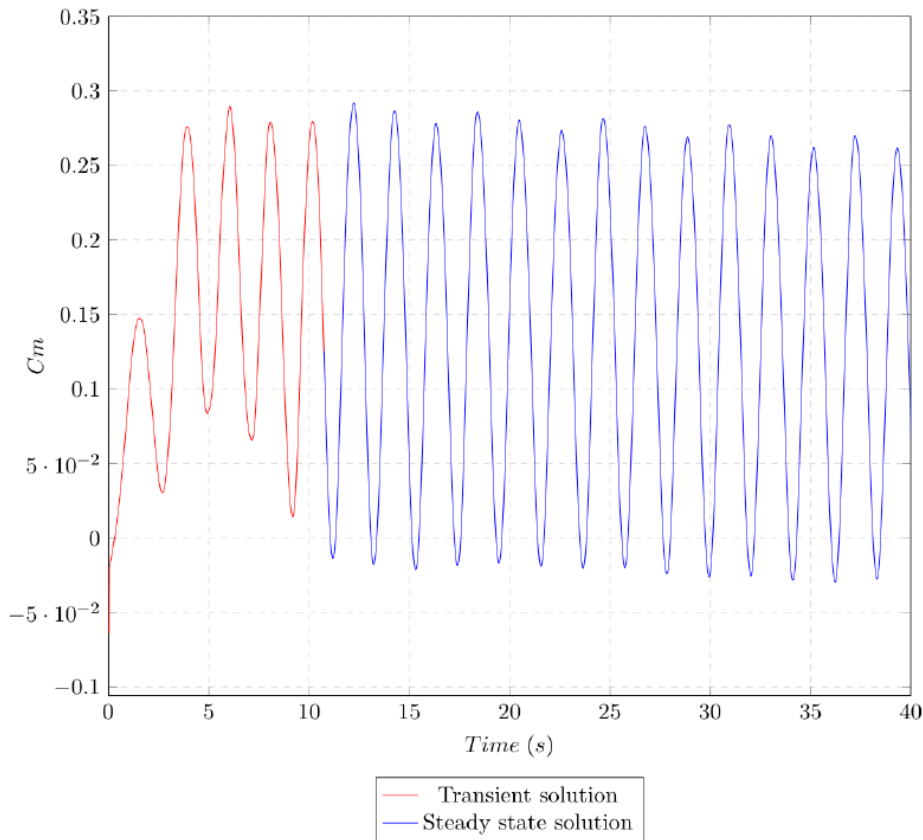
Figure 11: A typical figure of Moment coefficient as a function of time [65]

In the figure 11, two different types of pattern can be seen of which one in the initial portion seems like transient solution which is followed by a steady state pattern that is converged. The transient part has to be eliminated or ignored when we calculate the mean value of the function to get the ultimate moment coefficient value. However, the trimming of the unstable initial part is relatively a simple step whereas monitoring whether the solution is actually converged or not is a challenging part of the task.

As discussed in the previous paragraph, the mean of the different values in the steady state part is

found in order to get the ultimate turbine efficiency. And in this process of averaging, the transient effect part must not be included. Hence, the red colored part of the graph in figure 11 is ignored.

$$\overline{C_m} = \frac{1}{no.\,of\,samples} \sum_{i}^{n} C_m blade_i \qquad\qquad \textbf{\textit{Eq (3.39)}}$$

After obtaining the averaged moment coefficient, the turbine's power coefficient is determined using equation 3.38.

CHAPTER 4: CFD SIMULATION ENVIRONMENT

4.1 FLUID-STRUCTURE INTERACTION

Every object is surrounded by fluid in the environment. In this project, the H-Darrieus VAWT is surrounded by air. By fluid structure interactions, it is meant the interaction of any movable or deformable structure with an internal or surrounding fluid flow. The problems of fluid structure interaction (FSI) are some of the most important problems to solve. Considering computational and modelling issues, these are also some of the most challenging problems to deal with. [66]

The examples of finite structure interaction are all around us and it can be seen in medicine, science and engineering. The examples include fluttering of the wings of the aircrafts, falling of a leaf, the deflection of tidal or wind blades, blood pumping by the ventricles of the human heart, inflation of automobile airbags, or the motion of a Ship etc. [67]. This shows that in so many different fields, the fluid structure interaction problems have a very wide range of applications, such as automotive, biomedical, power generation, aerospace etc. among many other fields.

Fluid-Structure Interactions are an essential consideration when designing many engineering systems, since failing to consider the effects of oscillatory interactions, for example, could lead to disastrous results. This is a point which is focused in structures encompassing materials prone to fatigue, and the first Tacoma Narrows Bridge (1940) can be considered as a perfect instance of large-scale failure [68]. However, aircraft turbines and wings are also prone to breaking because of FSI vibrations or oscillations.

As a result, FSI analyses play an important role in a wide range of engineering and scientific domains. FSI evaluations are critical for material selection and understanding fatigue's impact on fluid flow and structural features, leading to better designs; yet, due to their significant multidisciplinary and nonlinearity nature, a full research of such problems remains a difficulty. Analytical solutions to the model equations are virtually impossible to find in most FSI scenarios, and laboratory experiments are limited in scope. As a result, numerical simulations are utilized to investigate the basic physics of the complex interaction of solids and fluids. This was only achievable in recent years, when finite element approaches for each of the individual challenges had progressed to the point that the necessary computer power was easily available. [69].

To further taking an interest in the FSI cases, [70] can be looked into, where FSI evaluations were conducted out on an airplane wing and a paragliding, respectively.

The main objective of this thesis is to do a successful 2D simulation of H-Darriues VAWT along with the validation with the available experimental data existing in the literature. In this chapter, the key steps of CFD simulation starting from drawing of a simple CAD of the turbine to meshing, setting of the fluent solver etc. are elaborated.

A flowchart is shown showing the ordered steps of the work flow used in the thesis to generate the simulation results:
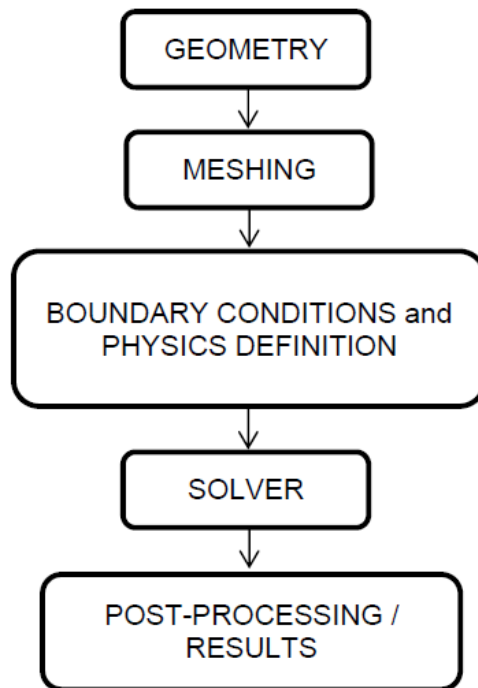
Figure 12:A Flow chart showing the steps of the CFD simulation

4.2 FEATURES OF THE EXPERIMENTAL ROTOR:

The experiment was conducted on a H-Darrieus VAWT whose height is 3m and diameter is 2.5 m. The airfoil profile of the blades is of NACA 0015 with a chord length of 0.4 m. the experiment was conducted on wind tunnel where the wind speed, hence the TSR was gradually increased sequentially and many readings were taken. [71]

The features of the rotor used in the experiment by [71] is illustrated below in the table:

Table 5: Features of the experimental rotor

Features	Rotor
Airfoil profile of blades	NACA 0015
Blade number	3
Blade length	3 m
Radius (R)	1.25 m
Blade chord (c)	0.4 m
Wind speed (V_w)	6 – 16 m/s (simulated for 10 m/s)
Speed of rotation (n)	20 – 150 (rev/min)
Tip Speed Ratio (λ)	0.2 - 2.2

Because no information on the shaft was available, the rotors' CAD was simplified by removing the shaft and modelling only the blades. To accurately compare numerical results with experimental ones, the experimental data were extrapolated in terms of C_p against λ curves.

4.3 DESIGNING THE TURBINE GEOMETRY

A crucial part of the modelling process is determining the appropriate computational domain for a Fluid Dynamic issue. It is vital to consider a variety of requirements. [72],[73].

To begin with, the domain must not be too limited to accurately duplicate the flow around the rotor, nor should it be too large to wastefully increase the grid's cell number and therefore computing time. Besides that, the domain must be capable of reproducing the rotation accurately. Finally, the meshing demands in regards to quality as well as the first cell placing near the blades must be considered.

The first step in starting a CFD simulation is to construct the geometry of the model that will be studied. The Design Modeler is an ANSYS tool for this purpose, however other CAD applications can be used to design the geometry and then imported into ANSYS to begin the meshing step.

This thesis made use of the Design Modeler tool. A comprehensive 3D geometry of the model was not viable due to the high computing cost, which would significantly increase the time required to accomplish this project. As a result, a 2D simulation was developed.

The coordinates of the airfoil from the leading edge to the trailing edge were collected from [74] in order to generate the turbine shape with Ansys Design Modeller. This airfoil was chosen since it is the aerofoil of the experimental turbine [71]. These airfoils will also be the turbine blades, which are the most important component to consider while constructing a turbine. The following stage is to read the file holding the airfoil coordinates and then generate the ultimate turbine geometry utilizing various options like resizing, translating, and scaling. It is important to note that the chord is 400 mm long.
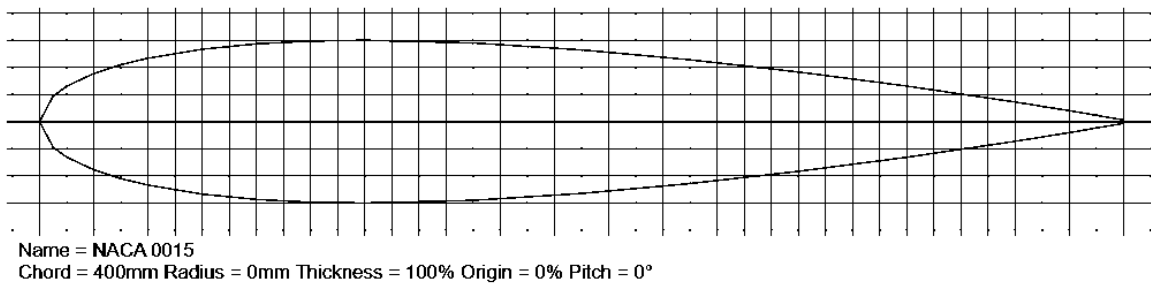

Figure 13: NACA 0015 obtained from aerofoil plotter [74]
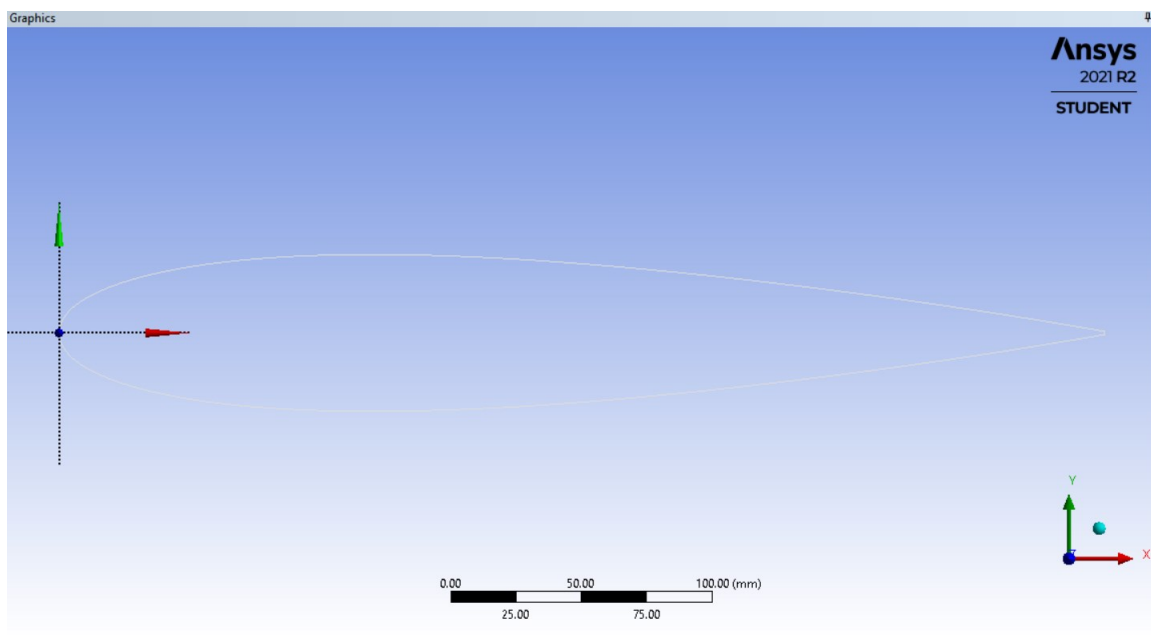
Figure 14: NACA 0015 aerofoil imported in the design modeler

The four-digit series includes NACA 0015. The NACA four-digit wing sections, according to Wikipedia, define the profile as follows:

1. The first digit denotes the maximum camber expressed as a percentage of the chord.

2. The second value represents the maximum camber from the leading edge of the airfoil in tenths of a chord.

3. The last two digits represent the airfoil's maximum thickness as a percentage of the chord.

The NACA 0015 aerofoil is symmetrical, with no camber indicated by the 00. The number 15 denotes a thickness-to-chord-length ratio of 15%: the airfoil is 15% thicker than it is in length. [75] NACA 0015 is a symmetrical NACA aerofoil that has been used in simulations as well as the experiment's turbine. Furthermore, it is mentioned in references as an excellent option for VAWT. [76]. Additionally, the use of symmetrical aerofoil simplifies the turbine's production process and lowers its expenses.

The center shaft and blades holding arms of the turbine were not considered in the simulation due to the turbine's simplicity of design. Lastly, all geometries created use the turbine's center as the main coordinate system's origin to make the Fluent application's results collection process easier. The geometry of the three-bladed VAWT is given in Figure 15 and 16:
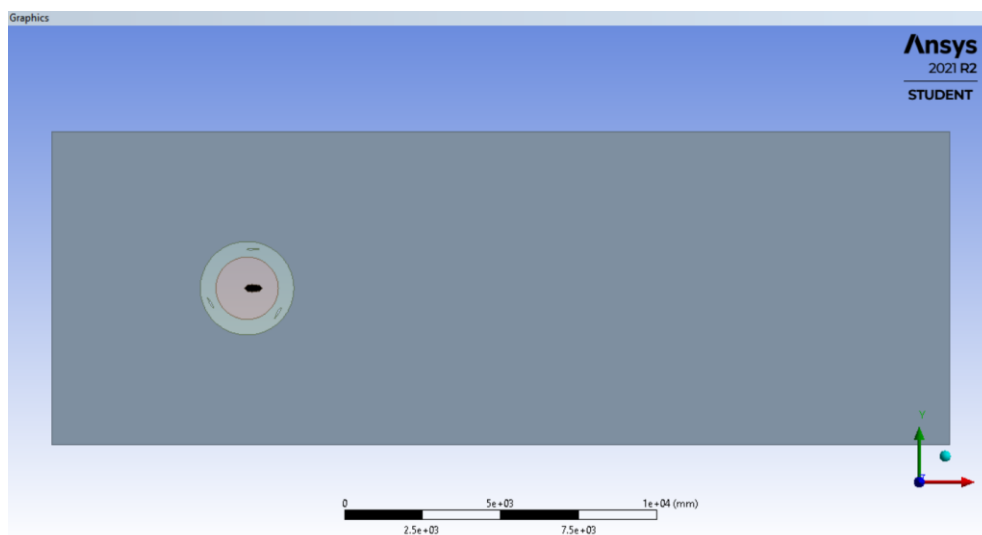
Figure 15: Geometry of the H-Darrieus VAWT drawn in design modeler for simulation
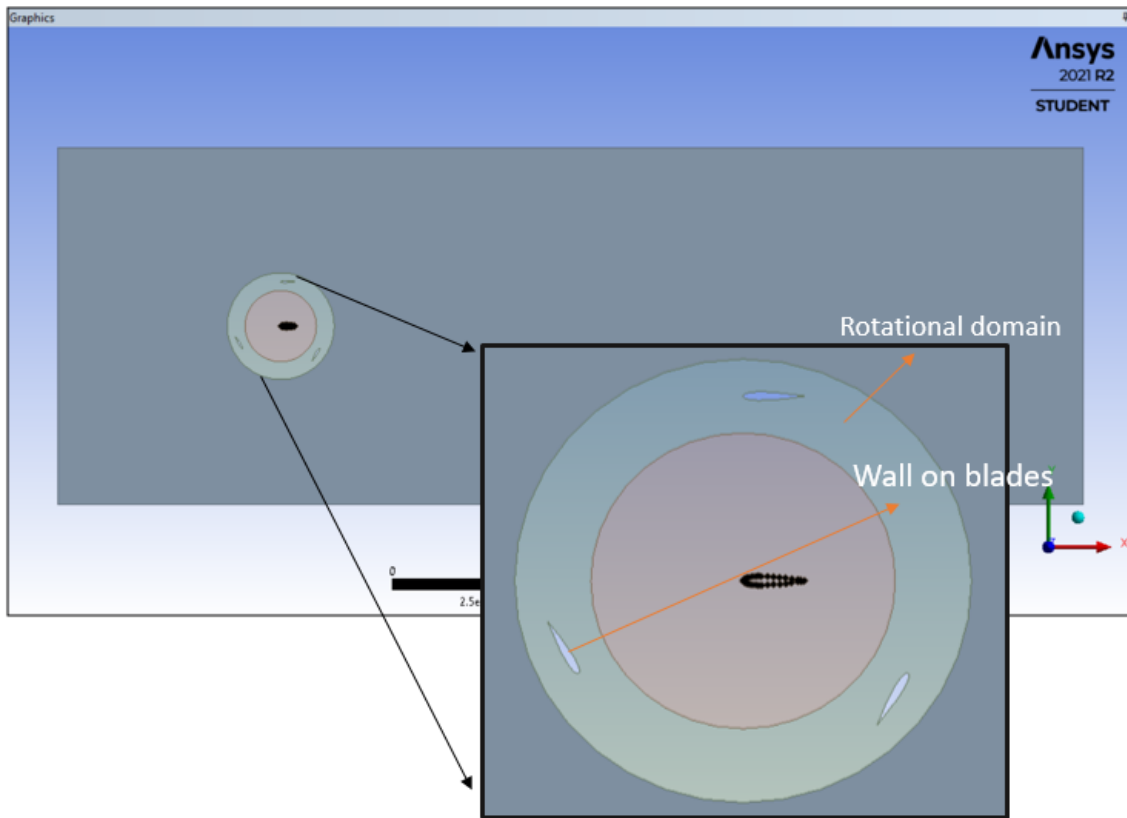
Figure 16: Geometry of the three bladed H-Darrieus VAWT

To use the Unsteady Sliding Mesh Model, the domain has three independent sub-domains. The ring is the only thing that moves, while the box and the interior circle remain motionless. The spinning ring must be as narrow as possible in the radial direction in order for the mesh motion to have no effect on the wake's true flow field. To accurately duplicate the wake effect, the rotor was situated five radii from the inlet and eighteen radii from the outlet. The distance between the top and bottom surfaces is four radius distance from the center. Using a domain that is excessively large will not result in improved results, but will instead result in an increase in cell numbers and, consequently, in processing time.

4.4 GENERATION OF MESH

In a CFD simulation, the second step is to discretize the entire domain that is being investigated. It's a crucial component, and it might also be the most difficult. The fluid dynamics governing equations are solved by meshing the domain, which is done by splitting it into many cells. A mesh independent solution must be achieved in order to produce a valid solution, which means that the findings gained do not vary despite mesh refinement. As a result, a mesh independence study has been included, which is detailed in a later section.

In this project, triangular mesh was created, as shown in figure 17:
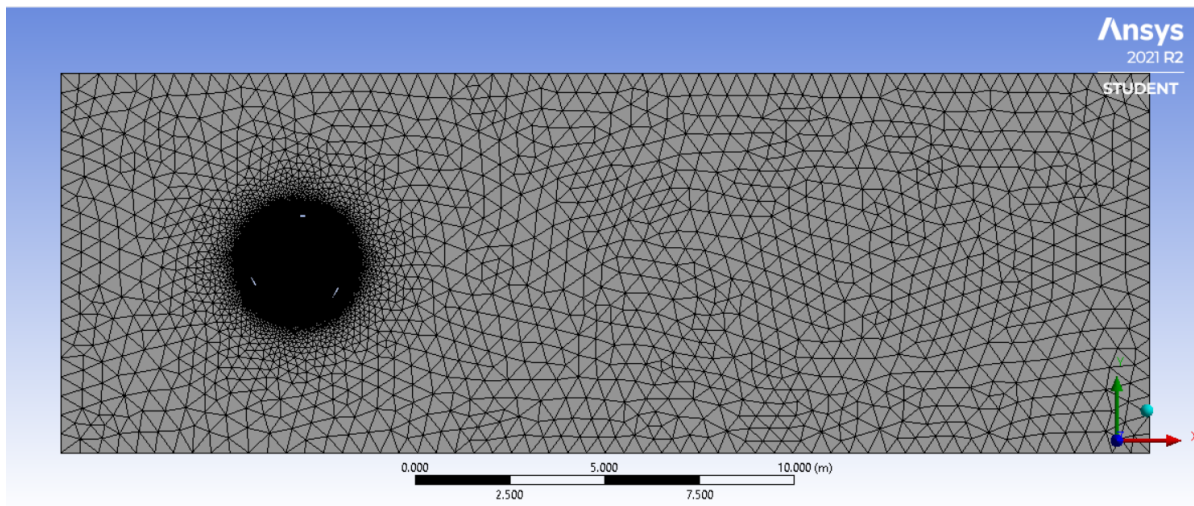
Figure 17: The fluid domain's mesh

The ring zone containing the airfoils is the zone with the highest density of elements, as can be observed. As previously indicated, this is the zone where the fluid characteristics change the most, so it is acceptable to use a denser mesh here.

Figure 18 demonstrates a zoomed picture of the mesh in the ring zone and around the airfoils:
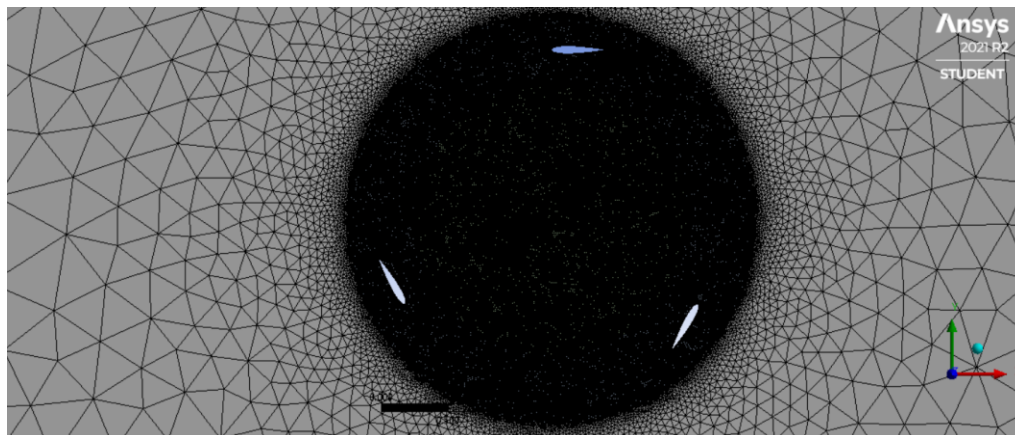
Figure 18: The Ring Zone's mesh

Figure 18 shows that the margins of the airfoil are really more refined, in order to capture the boundary layer effect and the larger velocity and pressure gradients that occur around the airfoil. ANSYS Meshing advance sizing methods were used to build a high-quality non-conforming unstructured mesh. In the boundary layer of the blades, an inflation tool has been used to construct 20 levels of quadrangular cells so that the y+ 1 as needed by turbulence models. [77][78] Outside the boundary layer, triangular cells were employed with the same growth rate up to the inside and outside interface. To reduce non-conformal mesh interpolation errors, triangular cells at the interfaces have the same dimensions for the three sub-domains.

After the meshing is complete, the named selections must be created. To make setting up the boundary conditions easier, the different portions of the domain must be designated.
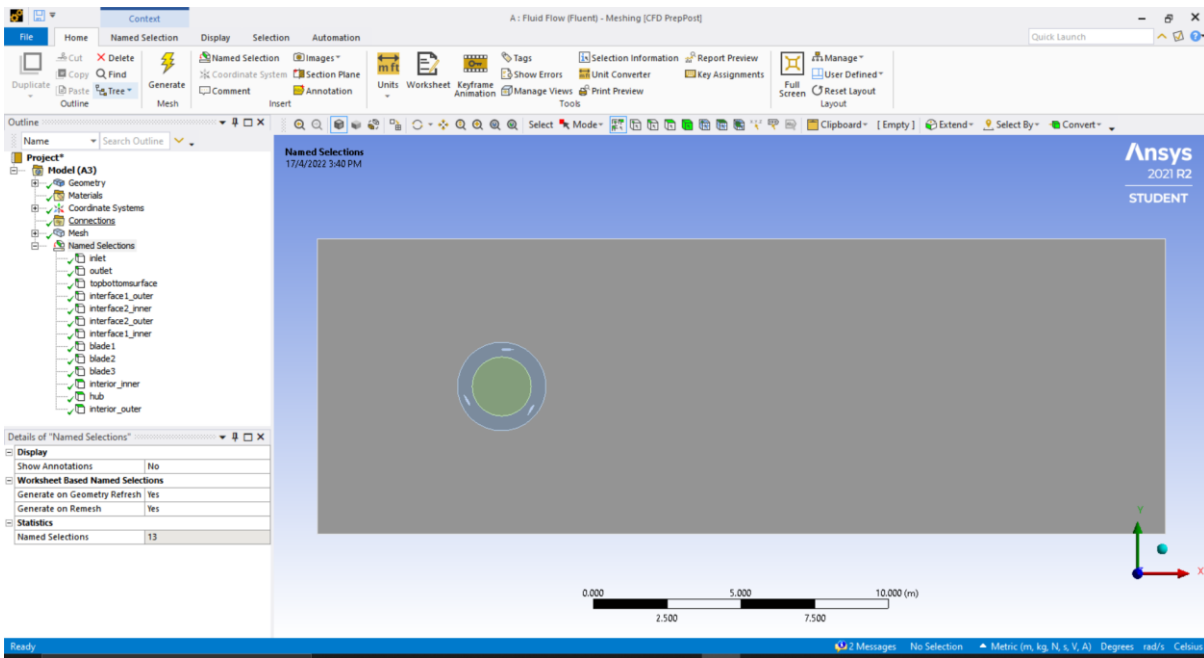
Figure 19: Named selection list at the left side of the figure
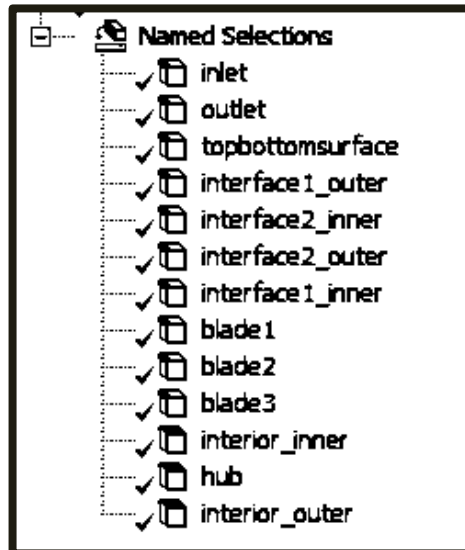
Figure 20: Named selection list

4.5 SOLVER SETTINGS- FLUENT SETUP

The simulation setup must be completed after the meshing procedure is completed. It may be sufficient to discuss the approach used to solve the unsteady flow around the VAWT before going into how the different simulation settings were established. In reality, a variety of strategies can be utilized to simulate this erratic flow. [79].

A sliding mesh approach was utilized to model the turbine's rotation.[80]. A portion of the mesh changes with time according to the rotational velocity required in each simulation in this type of simulation. As a result, in Fluent, a transient simulation is utilized to rotate the mesh, with a time step set. The rotating and fixed domains are linked by an interface, which assures that the flow properties of cells in different domains are transferred accurately.

4.5.1 The Sliding Mesh Approach

When calculating an unsteady flow field, the Sliding Mesh approach should be utilized if a time-accurate solution is needed. It's the most precise way for simulating flows in moving reference frames, but it's also the most time-consuming.

This method employs two or more cell zones, each of which is separated from the opposing cell zone by at least one 'interface zone.' A grid interface is formed by connecting the interface zones of adjacent cell zones, and the two cell zones will move relative to each other along the grid interface. [80]

In this study, the interfaces required for our modelling have already been created, and so this process is explained later.

4.6 SOLUTION SETUP

This part covers the setting and setup of the Fluent application used in this thesis' simulations, as well as the numerical solver and turbulence model choices, among other aspects.

As a solver, a pressure-based option is used. When dealing with incompressible flows, the Fluent user guide suggests it. [81]. At the same time, due to the flow's unpredictability, a time-dependent solution is necessary. [82]. As a result, depending on the time step value, the rotating mesh moves in discrete steps relative to the stationary mesh during the calculation.

4.6.1 Boundary Conditions

The next step in the simulation process is to define the system's boundary conditions after the geometry and mesh have been created. A velocity inlet on the left side that replicates air flow and a pressure outlet on the right side make up these boundary conditions.

The input velocity is compelled to be parallel to the x-axis, but its magnitude is determined by the fluid used. According to the experimental study, air simulations were done at a standard speed of 10 m/s.

On the top and bottom part of the simulation surface, the two walls are there where symmetry condition was applied. The velocity inlet and pressure outlet boundary conditions is recommended by *Fluent* [81] at the inlet and outlet of the simulation area which is used while simulating incompressible flows just like the present study when the Mach number is quite smaller than the values where compressible flow occurs.

It is critical to choose boundary conditions carefully in Fluent since they are necessary to attain a plausible solution. As a result, the physical events that relate to our simulation must be thoroughly investigated before defining the simulation model's boundary conditions.

The turbine blades are positioned in a revolving domain. As previously stated, an interface must be created in order to divide the rotating and stationary domains. There are two transitions between rotational and stationary domains in the simulations, hence two separate interfaces must be constructed. It's worth noting each interface connects two different cell zones, which is why each interface has two named selections in each cell zone.

Mesh Interface	Interface Zone 1	Interface Zone 2
Interface_1	Interface1_inner	Interface1_outer
Interface_2	Interface2_inner	Interface2_outer

The interface definition procedure is a critical part of the Fluent setup process, and an incorrect definition will result in unrealistic outcomes. This occurred during the initial simulations, when the average moment coefficient was negative for every range of tip speed ratio values simulated. The mass flow quantity was investigated on both sides of the cell zones separated by an interface, as advised by [82].

This parameter must be the same on both sides due to the continuity equation [83]. The discrepancy revealed that there was a problem with the interfaces, and that information was not being transmitted correctly between cells belonging to different cell zones. To fix the problem, the interfaces were erased and recreated.

4.6.2 Turbulence Model

Depending on the nature of the case to be studied, Fluent permits the use of various turbulence models. The Shear Stress Transport (SST) was used in this instance, as it was in most of the publications identified about VAWT. The SST turbulence model is a four-equation model that combines the two-equation models k-ε and k-ω. [84] shows that SST gives better values for the kind of flow expected in VAWT. The default values for Fluent have not been changed.

4.6.3 Time Step Calculation

A transient simulation, as previously stated, needs the application of time-dependent calculations. In the case of a sliding mesh problem, this time step determines how many degrees the mesh revolves in each computation based on the turbine's imposed rotational velocity. Instead of dealing with the time step value, the relation between the degrees of rotation of the sliding mesh each time step was used because it proved to be a more straightforward and comprehensive parameter. The relationship between these two parameters is stated in the following paragraphs:

This procedure begins with the turbine's rotational velocity being set. The next step is to calculate the time required to spin one degree, taking into consideration the radian-to-degree relationship:

$$\omega = \frac{\Delta\theta}{\Delta t} \qquad\qquad Eq\ (4.1)$$

$$\Delta t = \frac{\Delta\theta}{\omega} \qquad\qquad Eq\ (4.2)$$

$$\Delta t|_{1°} = \frac{1}{\omega(rps).\,360} \qquad\qquad Eq\ (4.3)$$

The relationship between the time step and the rotational velocity is significant to observe from the previous equation. This means that the time step must be adjusted for the entire range of tip speed ratio values out of which turbine performance is calculated.

In chapter 5, a time independence study explains how to choose the right time step size.

4.6.4 Reference Values and Power Coefficient

The reference values used for computing normalized flow field variables such as moment, moment coefficient etc. can be set in Fluent: [61]

$$C_p = \frac{P_t}{P_a} = \frac{M\omega}{\frac{1}{2}\rho A v^3} \qquad\qquad Eq\ (4.4)$$

The total moment M is calculated in Fluent using the moment coefficient Cm, which is stated as:

$$C_m = \frac{M}{\frac{1}{2}\rho A v^2 L} \qquad\qquad Eq\ (4.5)$$

A is the reference area, and L is the reference length in the equation above.

With these considerations in mind, the power coefficient equation can be reduced to the following:

$$C_p = \frac{C_m \frac{1}{2}\rho v^2 A L \omega}{\frac{1}{2}\rho A v^3} = C_m \frac{\omega L}{v} \qquad\qquad Eq\ (4.6)$$

In 2D simulations of turbines, the value of A is equal to the diameter of the turbine, while the value of L is equal to the radius of the turbine, as detailed in [85]. When these adjustments are applied to equation 4.6, the following equation is obtained:

$$C_p = C_m \frac{\omega R}{v} \hspace{3cm} \textit{Eq (4.7)}$$

Lastly, a simple statement can be derived that links the power coefficient with the tip speed ratio and the moment coefficient extracted by the Fluent models by applying the definition of the tip speed ratio from in equation 4.7:

$$C_p = C_m \lambda \hspace{3cm} \textit{Eq (4.8)}$$

Apart from the geometric reference values, which are only dependent on the turbine size, there are other fluid-related characteristics such as density and viscosity. All of the reference values in the simulations were calculated using the inlet boundary condition, which forces the value of the free stream velocity. The primary reference values for the Vertical axis wind turbine simulations are listed in Table 7. Once the fluid is established in the Materials dialog box in the Problem Setup menu, these values can be set automatically or manually by the Fluent materials database.

Table 7: Reference Values

Parameters	Values (a)
Velocity	10 (m/s)
Viscosity	1.7894e-5 (kg/m-s)
Density	1.225 (kg/m^3)
Length (m)	1.25 m (Turbine Radius)
Area (m^2)	2.5 m (Turbine Diameter)

4.6.5 Solution Methods

Several Fluent solver algorithms were examined, and the simulated parameters such as the moment coefficient showed little variation. However, the PISO Pressure- Velocity Coupling method was chosen based on the major guidelines provided in the Fluent Theory Guide [86] as Fluent recommends it for transient or unsteady simulations.

In Fluent, the next step is to choose the Spatial Discretization methods:

▪ Gradient: For unstructured meshes, the Fluent Theory Guide advises using the Least Squares Cell Based method.

▪ Pressure: Second order method is used for transient simulations.

- Momentum: Instead of using First Order Upwind, which could provide a faster convergence, Second Order Upwind is employed for better accuracy.
- Transient Formulation: Second Order Implicit method was used for better results

The remaining parameters are set to their default values in Fluent.

4.6.6 Summary of the fluid domain simulation

Table 8: Summary of the fluid domain simulation

Geometry	Airfoil	NACA 0015
	Turbine diameter D (m)	2.5
	Turbine radius R (m)	1.25
	Chord length c (m)	0.4
	Number of blades	3
Solver	Turbulence model	Transition SST
	Approach	Sliding Mesh
	Pressure-Velocity Coupling Scheme	PISO
	Gradient discretization	Least Squares Cell Based
	Pressure discretization	Second Order
	Momentum discretization	Second Order Upwind
	Turbulent Kinetic Energy discretization	Second Order Upwind
	Specific Dissipation Rate discretization	Second Order Upwind
	Momentum Thickness Re discretization	Second Order Upwind
	Transient Formulation	Second Order Implicit
Reference values	Free stream velocity V_∞ (m/s)	10
	Density ρ (kg/m^3)	1.225
	Dynamic viscosity μ (kg/m $\cdot$ s)	1.7894e-05
Other parameters	Time step	$\Delta t|_{1°}$
	Max. Iterations per time step	60
	Number of time steps for 1 revolution	360

CHAPTER 5: RESULTS AND DISCUSSIONS

After detailing the configuration process of Fluent, this chapter presents the results obtained in the simulations that have been carried out. In these simulations, the moment coefficient average was obtained at different tip speed ratios. Then one point was obtained running simulations at one particular turbine rotational speed. This way, a C_p vs λ curve was obtained. Then validation of the simulations was done by comparing this result with the existing experimental data.

Prior to running the final simulations to obtain the C_p vs λ curve, two important studies were done, namely mesh independent study and time independent study.

First, mesh independent study is discussed which is related to the study about the size of the mesh and this study is a key factor for any CFD simulation. Then, the time independent study is discussed which involves setting up an optimum time step size for the simulations.

5.1 MESH INDEPENDENCE STUDY

The meshing is one of the most important steps in CFD simulation. Majority of the time and effort is spent in this step in the CFD industry.

It is needless to mention to understand that the finer the mesh is, the better is the result that can be expected to obtain. However, the finer the mesh is, the higher is the number of elements and nodes. So reducing the cell element size will increase the computational effort and high time will be needed to reach a final solution. So, a trade-off always has to be made between the computational cost and the precision of the simulation results.

In order to work with an optimum mesh size, prior to running the final simulations, a mesh or grid independent study is an obvious step to do. This study starts with an approximate mesh designed for the current case. Then evaluation of a variable of interest is done as the mesh gets finer and finer. As the mesh gets finer, the result obtained from the finer mesh is more precise than that of the coarse mesh. This way, mesh is kept making finer and the process is iterated until the difference between the results obtained from one mesh reduces up to a desired value than that of the previous mesh. This is what can be considered as reaching convergence from a mesh point of view. After this convergence is reached, there is no need to make the mesh finer as it would provide us results with satisfactory precision without unnecessarily increasing computational time.

In this study also, a mesh independent study is done. However, the study has limitation with high relative error that is discussed later. The Mesh is numbered as 1-4 to help denoting them according to the trial sequence during simulation trial running. The mesh numbers with their cell and node numbers and obtained C_p value are tabulated here:

Table 9: Mesh Independence Study

Mesh number	Mesh elements	Mesh nodes	C_p
1 (coarser)	21003	12588	0.561592
2 (coarse)	53986	29558	0.331163
4 (fine)	169453	88105	0.198941
3 (finer)	204341	105723	0.155188

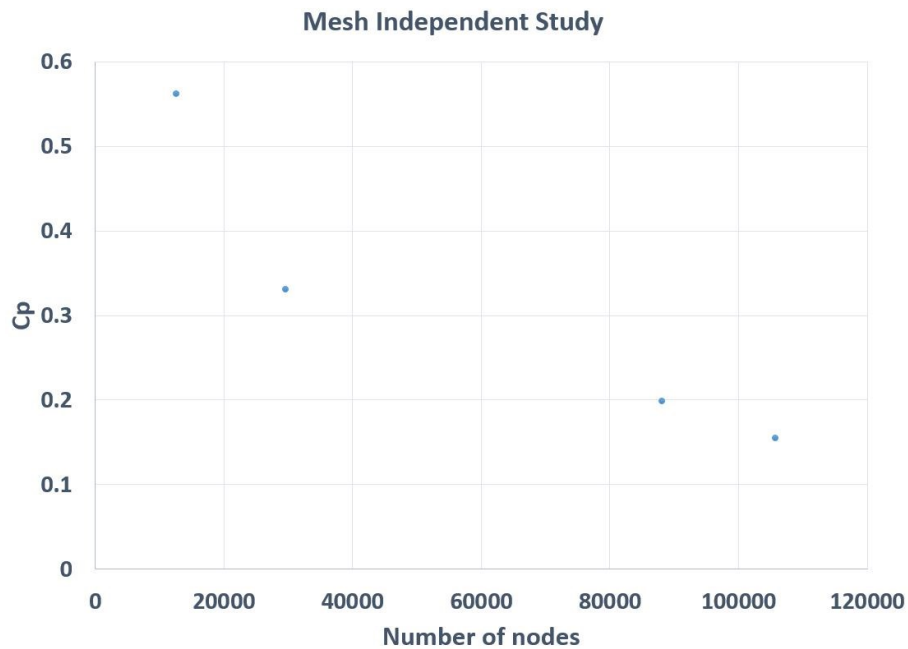Graphically, the obtained result is also shown:

Figure 21: Power coefficient as a function of number of nodes

The mesh independent study conducted here has severe limitations that may even lead to unsatisfactory endings. The relative error of C_p obtained is considerably high. Only the mesh which matched best with the simulation result was ultimately selected (Mesh 3) due to lack of computational capacity and time. However, this is a serious limitation that should be attended in the future attempts.

The mesh independent study needs more trials approach which could not be done here as computational time for this type of transient simulation with the available design is very high (more than 15 hours per simulations). Use of a device with higher computational capacity may help resolve this issue.

5.2 TIME INDEPENDENCE STUDY

As it was shown in the previous section, the time step calculation was done accordingly. To validate the result, numerous tests were done to get an optimum time step value for the simulation prior to conducting the final simulations. When the time step value is high, it is associated with high mesh displacement. So, a high time step value could lead to a non-converging solution. Conversely, if the time step size is low, it ensures convergence of the solution. However, low time step size increases the simulation time, and sometimes, with no noteworthy difference in the final solutions. So, there a compromise is to be made between the maximum time step size and the total simulation time.

Five time step sizes were tested to evaluate their influence over the result. Keeping a constant 98 rev/min turbine angular velocity, the simulations were run at different time step sizes. To have a better understanding of the phenomenon, the angle of rotation of the mesh per time step was used primarily and then additional smaller time steps were included in the trials. The results are tabulated in table 10:

Table 10: Time Independent Study

Rotation/time step	Time step value (second)	C_p	Relative error
-	0.0004	0.115454	-
-	0.0005	0.136025	15.12
1˚	0.0017	0.292647	53.51
2 ˚	0.0034	0.363943	19.59
2.5 ˚	0.00425	0.33116	9.899
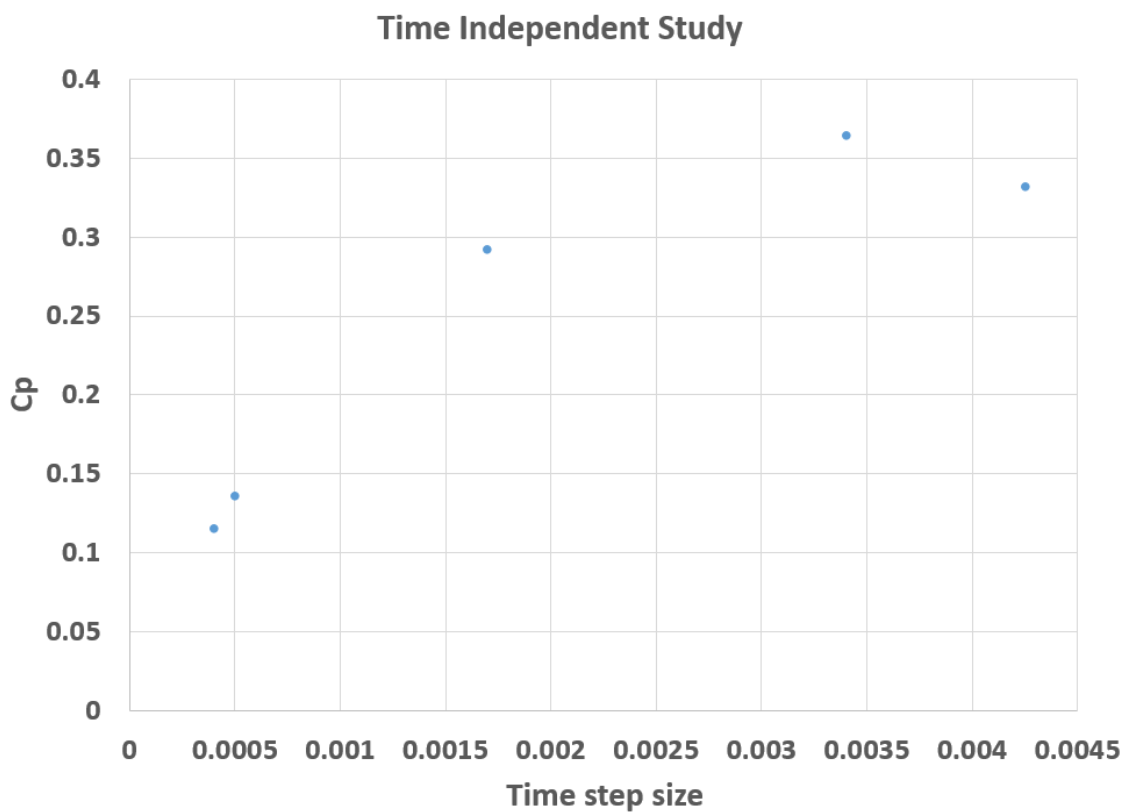
Figure 22: Power coefficient as a function of time step size

From the table and graph, it can be seen that the values for .0004 s and .0005 s are considerably close. These values are nearer to the experimental value which was checked. However, .0004s time step size is very low increasing the computational time. On the other hand, the relative error is very high between the time step size .0005 s and .0017 s. So ultimately, .0005 s was selected as the optimum time step size.

However, just like the mesh independent study, the time independent study also would have required more trials which could not be done due to limitations as previously mentioned.

5.3 VALIDATION OF SIMULATION WITH DATA PRESENT IN THE LITERATURE

5.3.1 C_p vs λ Curve

In this study, the validation of the simulation is done using the C_p vs λ curve available in the existing literature [71]. The Power coefficient is calculated as mentioned in the previous section by averaging the moment coefficient and multiplying the average moment coefficient with the tip speed ratio (TSR). Although the results show some discrepancy, the curve obtained by the simulated results matches considerably with the experimental curve as shown in the figure:
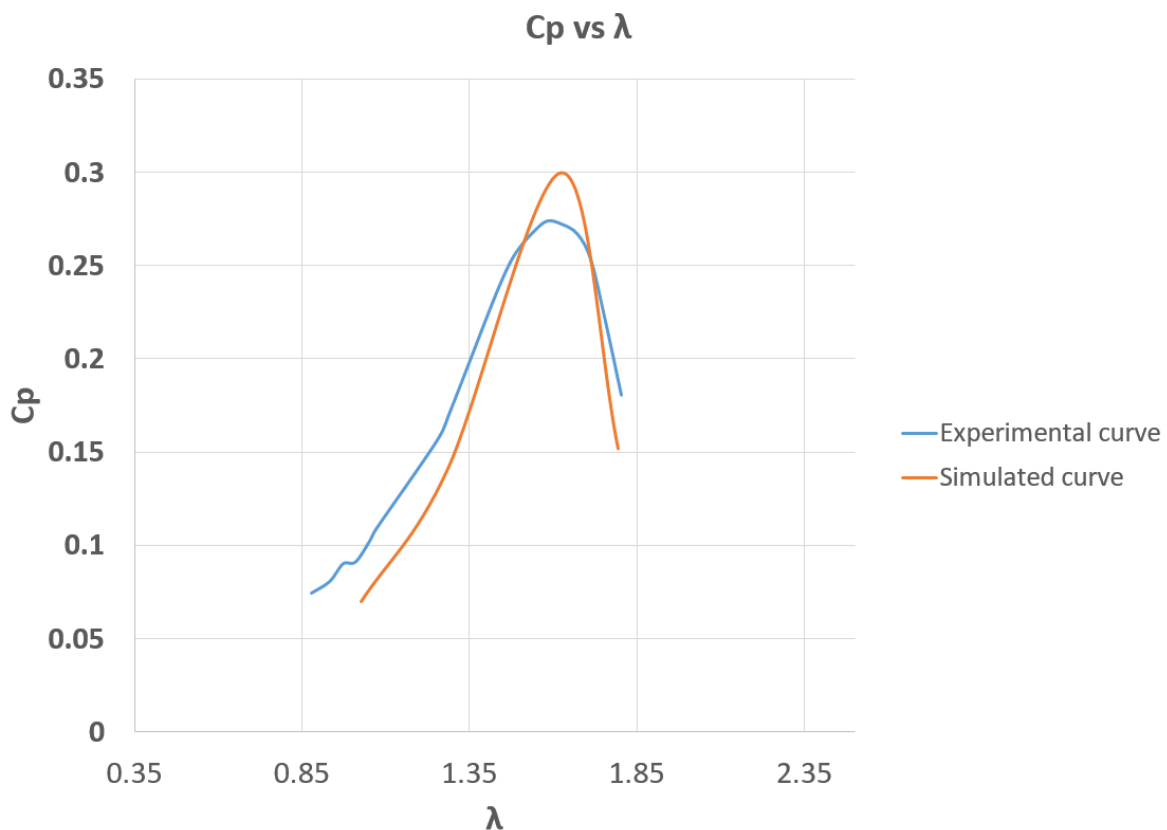
Figure 23: Validation of the simulation with C_p vs λ curve

5.4 VELOCITY FIELD PLOTS

The simplest and easiest assumption that can be made about the flow-field across a VAWT is to consider uniform velocity of 10 m/s across the turbine. But in reality, this is not true as it can be seen from the velocity contour in figure 24 and figure 25.

The magnitude of velocity starts to decrease as wind flows near the VAWT rotor. At the blades' trailing edge, the magnitude of wind velocity remains the lowest. After striking the wind at the

rotor blade, the wind also generates some angular velocity and hence begins to gain velocity again.

Generally, at leading edges of the turbine blades, and mainly on the pressure sides of the blade, regions of higher velocities are observed. The lowest velocities are usually observed at the back side of the rotors, which always creates a vacuum.

Figure 24: Velocity contour plot
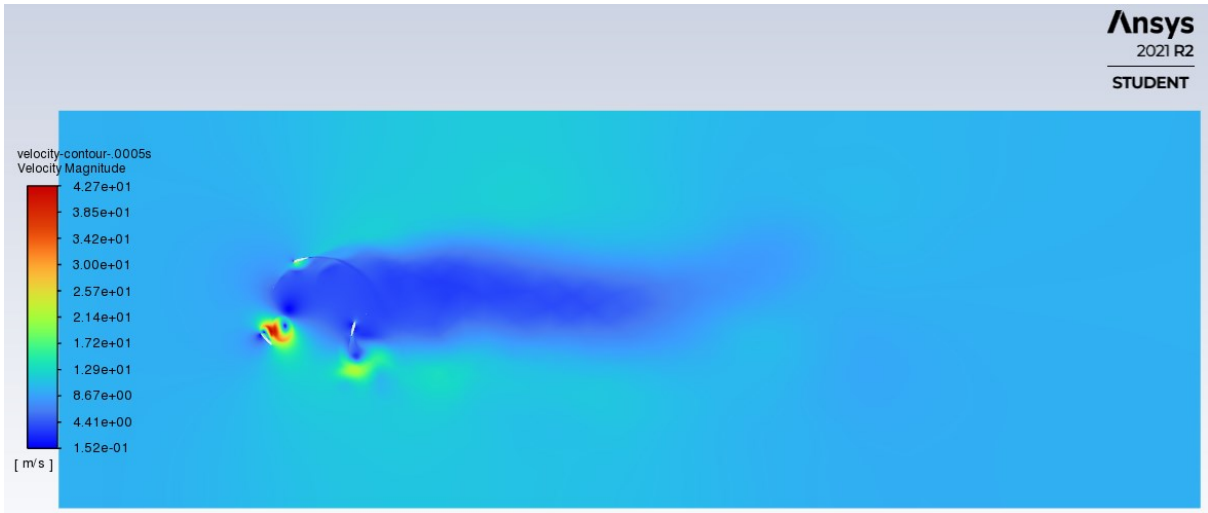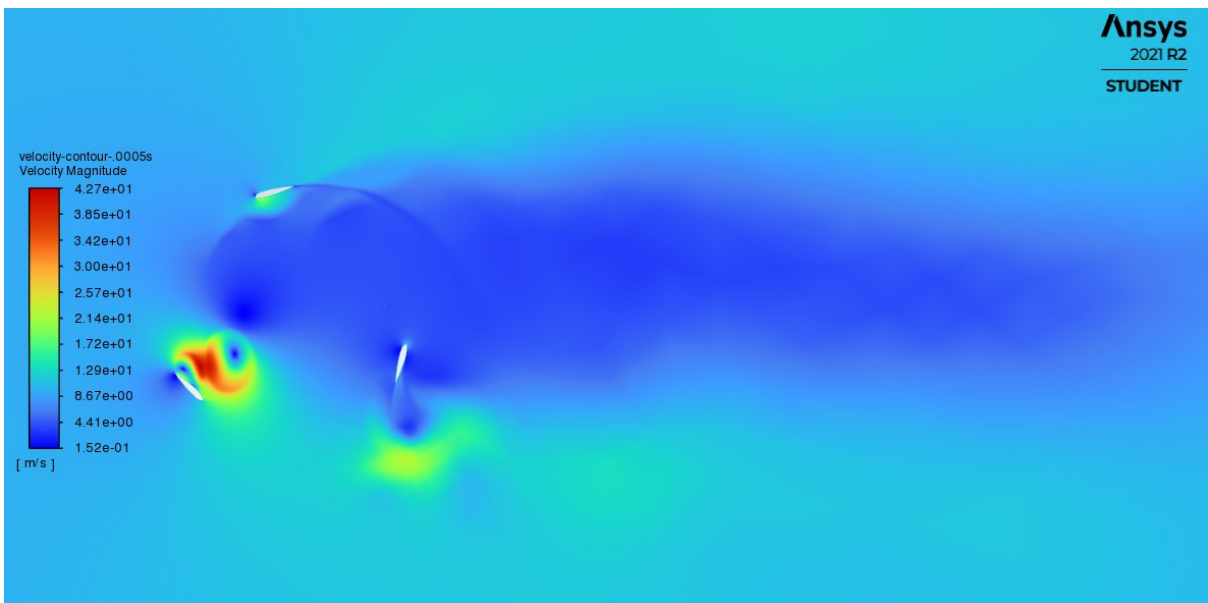

Figure 25: Velocity contour plot (zoomed)

CHAPTER 6: CONCLUSIONS AND RECOMMENDATIONS

6.1 SUMMARY OF THE WORK

In this thesis, a 2D simulation of a H- Darrieus Vertical Axis Wind Turbine is done using one of the most popular CFD software package, namely, ANSYS. Several simulations were run at different tip speed ratios. The moment coefficient was obtained from these simulations. The moment coefficients obtained at different time steps were then averaged for up to two revolutions in the steady state of the turbine rotation. Then the obtained average power co-efficient is multiplied by the corresponding tip speed ratio. And thus power coefficient of the corresponding tip speed ratio was obtained. In this way, the results obtained were used to draw a performance curve. One of the main objectives of this thesis is the validation of the simulated result. The validation was done with results of a study available in the literature.

Cp vs λ curves can be used in wind turbine design to determine the rotor power for any combination of wind and rotor speed. They provide immediate information on the maximum rotor power coefficient and optimum tip speed ratio.

The Cp vs λ curve of the literature was compared with the one obtained from the simulated results. Thus validation of the simulation was done which shows the results match considerably.

Prior to the simulation, two important studies were done. One is mesh (grid) independent study another one is the time independent study. Both the studies are very important to get a good result from the simulation sand also to obtain results with optimum computational effort with efficiency. This efficiency reduces both computational cost and time.

6.2 CONCLUSION

Lastly, it can be concluded that:
- In this project, the 2D simulation of a H-Darrieus VAWT was done using Computational Fluid Dynamics (CFD) simulation software Fluent.
- Cp vs λ curve obtained from the simulation matches considerably with the experimental data.
- Sliding Mesh model was used which takes into account the vortices generated by the blades

passing upwind on the blades downstream unlike over-simplified MRF model.

- Prior to the simulation, mesh independent and time independent study was done not only to validate the result but also to reduce the computational effort
- This study can be used for design optimization and performance improvement of wind turbine

6.3 RECOMMENDATION AND FUTURE WORKS

This thesis has many limitations that should be attended to gain better accuracy of the simulation works. In this thesis, only simulation with validation is done with the intention of doing further studies on the performance evaluation of wind turbine. This thesis is just a simple initial endeavor that is expected to contribute in the development of higher order simulations in the future. Some limitations with recommendations to attend them are mentioned here:

- In this project, only simulation with validation is done with the intention of doing further studies on the performance evaluation of wind turbine. It is recommended to do further studies like studying the effect of using different blade profiles, studying the effect of turbine radius and chord length etc.
- 2D simulations has its limitations as it doesn't consider 3D effects like tip vortex that leads to overestimation of generated power. So, the best results are expected to obtain by developing a 3D model which is recommended to develop.
- The mesh and time dependent study done here needs more trial and error attempts which could not be done due to time and computational limitations but is recommended and intended to do in the future.
- The simulation was done on a personal computer with low computational capacity. For running this type of transient simulations, a device with better capacity would be required and recommended.

This thesis has many limitations that are intended to be attended in the future endeavors. The future endeavor would include evaluating wind turbine performance parameters for example: the effect of different airfoils, the effect of chord length, the effect of turbine radius length etc. and the knowledge obtained from those simulations can help in the design optimization and improvements of H-Darrieus vertical axis wind turbines.

Also, to overcome the limitations of 2D model, a 3D model may be developed and used implementing higher computational power.

REFERENCES:

[1]   M. N. Uddin, M. A. Rahman, M. Mofijur, J. Taweekun, K. Techato, and M. G. Rasul, "Renewable energy in Bangladesh: Status and prospects," *Energy Procedia*, vol. 160, pp. 655–661, 2019, doi: 10.1016/j.egypro.2019.02.218.

[2]   P. Action, *Poor people's energy outlook 2016: National energy access planning from the bottom up*. Practical Action Publishing, 2016.

[3]   G. Plan, "Power Division, Ministry of Power, Energy and Mineral Resources, Government of the people's republic of Bangladesh." 2018.

[4]   Bangladesh Power Development Board, "Annual Report 2020-21," 2021. [Online]. Available:

https://bdcom.bpdb.gov.bd/bpdb_new/resourcefile/annualreports/annualreport_1640756525_ Annual_Report_2020-2021_latest.pdf.

[5]   Z. Tan, H. Zhang, J. Xu, J. Wang, C. Yu, and J. Zhang, "Photovoltaic power generation in China: Development potential, benefits of energy conservation and emission reduction," *J. Energy Eng.*, vol. 138, no. 2, pp. 73–86, 2012.

[6]   S. Ahmed, M. T. Islam, M. A. Karim, and N. M. Karim, "Exploitation of renewable energy for sustainable development and overcoming power crisis in Bangladesh," *Renew. Energy*, vol. 72, pp. 223–235, 2014, doi: 10.1016/j.renene.2014.07.003.

[7]   F. Ahmed, A. Q. Al Amin, M. Hasanuzzaman, and R. Saidur, "Alternative energy resources in Bangladesh and future prospect," *Renew. Sustain. Energy Rev.*, vol. 25, no. September, pp. 698–707, 2013, doi: 10.1016/j.rser.2013.05.008.

[8]   H. Akter, H. O. R. Howlader, A. Nakadomari, M. R. Islam, A. Y. Saber, and T. Senjyu, "A Short Assessment of Renewable Energy for Optimal Sizing of 100% Renewable Energy Based Microgrids in Remote Islands of Developing Countries: A Case Study in Bangladesh," *Energies*, vol. 15, no. 3, 2022, doi: 10.3390/en15031084.

[9]   H. Mohammad, "Achieving sustainable energy targets in Bangladesh," *UN Chron.*, vol. 52, no. 3, pp. 36–39, 2013.

[10]   W. Frost and C. Aspliden, "Characteristics of the wind. Wind Turbine Technology: Fundamental Concepts of Wind Turbine Engineering, DA Spera, Ed." ASME Press, 1994.

[11]   P. Gipe, *Wind energy basics: a guide to small and micro wind systems*. Chelsea Green publishing company White River Junction, VT, 1999.

[12]   P. K. Halder, N. Paul, M. U. H. Joardder, and M. Sarker, "Energy scarcity and potential of renewable energy in Bangladesh," *Renew. Sustain. Energy Rev.*, vol. 51, no. September 2017, pp. 1636–1649, 2015, doi: 10.1016/j.rser.2015.07.069.

[13]   A. Zervos, "Renewable Energy Policy Network for the 21st Century," *Renew. Energy Policy Netw. 21st Century*, pp. 1–367, 2020, [Online]. Available: http://www.ren21.net/pdf/RE2007_Global_Status_Report.pdf.

[14]   M. R. Islam, M. R. Islam, and M. R. A. Beg, "Renewable energy resources and technologies practice in Bangladesh," *Renew. Sustain. Energy Rev.*, vol. 12, no. 2, pp. 299–343, 2008.

[15]   M. S. Kaiser, M. A. Rahman, M. M. Rahman, and S. A. Sharna, "Wind energy assessment for the coastal part of Bangladesh," *J. Eng. Appl. Sci.*, vol. 1, no. 2, pp. 87–92, 2006.

[16]   R. Vijay, "Pitch Control of Horizontal Axis Wind Turbine Pitch," p. 42, 2011.

[17]   J. Liu, H. Lin, and J. Zhang, "Review on the technical perspectives and commercial viability of vertical axis wind turbines," *Ocean Eng.*, vol. 182, no. October 2018, pp. 608–626, 2019, doi: 10.1016/j.oceaneng.2019.04.086.

[18]   D. MacPhee and A. Beyene, "Recent advances in rotor design of vertical axis wind turbines," *Wind Eng.*, vol. 36, no. 6, pp. 647–666, 2012, doi: 10.1260/0309-524X.36.6.647.

[19]   M. Ghasemian, Z. N. Ashrafi, and A. Sedaghat, "A review on computational fluid dynamic simulation techniques for Darrieus vertical axis wind turbines," *Energy Convers. Manag.*, vol. 149, pp. 87–100, 2017, doi: 10.1016/j.enconman.2017.07.016.

[20]   G. Bedon, E. G. A. Antonini, S. De Betta, M. Raciti Castelli, and E. Benini, "Evaluation of the different aerodynamic databases for vertical axis wind turbine simulations," *Renew. Sustain. Energy Rev.*, vol. 40, pp. 386–399, 2014, doi: 10.1016/j.rser.2014.07.126.

[21]   A. A. Mohammed, H. M. Ouakad, A. Z. Sahin, and H. M. S. Bahaidarah, "Vertical axis wind turbine aerodynamics: Summary and review of momentum models," *J. Energy Resour. Technol. Trans. ASME*, vol. 141, no. 5, pp. 1–10, 2019, doi: 10.1115/1.4042643.

[22]   L. Du, G. Ingram, and R. G. Dominy, "A review of H-Darrieus wind turbine aerodynamic research," *Proc. Inst. Mech. Eng. Part C J. Mech. Eng. Sci.*, vol. 233, no. 23–24, pp. 7590–7616, 2019, doi: 10.1177/0954406219885962.

[23]   M. M. Aslam Bhutta, N. Hayat, A. U. Farooq, Z. Ali, S. R. Jamil, and Z. Hussain, "Vertical axis wind turbine - A review of various configurations and design techniques," *Renew. Sustain. Energy Rev.*, vol. 16, no. 4, pp. 1926–1939, 2012, doi: 10.1016/j.rser.2011.12.004.

[24] R. J. Templin, "Aerodynamic performance theory for the NRC vertical-axis wind turbine," National Aeronautical Establishment, Ottawa, Ontario (Canada), 1974.

[25] M. Islam, D. S.-K. Ting, and A. Fartaj, "Aerodynamic models for Darrieus-type straight-bladed vertical axis wind turbines," *Renew. Sustain. energy Rev.*, vol. 12, no. 4, pp. 1087–1109, 2008.

[26] R. E. Wilson and L. P.B.S., "MACHINES POWER WIND Of AERODYNAMICS," *Ntis Pb 238594*, no. Oregon State University, 1974.

[27] J. H. Strickland, "Darrieus turbine: a performance prediction model using multiple streamtubes," Sandia Labs., Albuquerque, N. Mex.(USA), 1975.

[28] R. J. Muraca, M. V Stephens, and J. R. Dagenhart, "Theoretical performance of cross-wind axis turbines with results for a catenary vertical axis configuration," 1975.

[29] D. J. Sharpe, *A theoretical and experimental study of the Darrieus vertical axis wind turbine*. Polytechnic School of Mechanical, Aeronautical and Production Engineering, 1977.

[30] S. Read and D. J. Sharpe, "An extended multiple streamtube theory for vertical axis wind turbines," in *Wind Energy Workshop*, 1980, pp. 65–72.

[31] F.-Z. Tai, K.-W. Kang, M.-H. Jang, Y.-J. Woo, and J.-H. Lee, "Study on the analysis method for the vertical-axis wind turbines having Darrieus blades," *Renew. energy*, vol. 54, pp. 26–31, 2013.

[32] S.-C. Roh and S.-H. Kang, "Effects of a blade profile, the Reynolds number, and the solidity on the performance of a straight bladed vertical axis wind turbine," *J. Mech. Sci. Technol.*, vol. 27, no. 11, pp. 3299–3307, 2013.

[33] I. Paraschivoiu, "Double-Multiple Streamtube Model for Studying VAWT's," *J. Propuls. Power*, vol. 4, no. 4, pp. 370–378, 1988, [Online]. Available: http://ci.nii.ac.jp/naid/80004153847/en/.

[34] H. Beri and Y. Yao, "Double multiple streamtube model and numerical analysis of vertical axis wind turbine," *Energy Power Eng.*, vol. 3, no. 03, p. 262, 2011.

[35] I. Paraschivoiu, F. Saeed, and V. Desobry, "Prediction capabilities in vertical-axis wind turbine aerodynamics," *World Wind Energy Conf. Exhib.*, no. October, pp. 3–6, 2002.

[36] J. H. Strickland, B. T. Webster, and T. Nguyen, "A vortex model of the darrieus turbine: An analytical and experimental study," *J. Fluids Eng. Trans. ASME*, vol. 101, no. 4, pp. 500–505, 1979, doi: 10.1115/1.3449018.

[37] L. B. Wang, L. Zhang, and N. D. Zeng, "A potential flow 2-D vortex panel model: Applications to vertical axis straight blade tidal turbine," *Energy Convers. Manag.*, vol. 48, no. 2, pp. 454–461, 2007, doi: 10.1016/j.enconman.2006.06.017.

[38] I. H. Hirsch and A. C. Mandal, "A cascade theory for the aerodynamic performance of Darrieus wind turbines," *Wind Eng.*, pp. 164–175, 1987.

[39] B. Hand and A. Cashman, "Aerodynamic modeling methods for a large-scale vertical axis wind turbine: A comparative study," *Renew. Energy*, vol. 129, pp. 12–31, 2018.

[40] B. Hand, A. Cashman, and G. Kelly, "A low-order model for offshore floating vertical axis wind turbine aerodynamics," *IEEE Trans. Ind. Appl.*, vol. 53, no. 1, pp. 512–520, 2016.

[41] A. Rezaeiha, H. Montazeri, and B. Blocken, "On the accuracy of turbulence models for CFD simulations of vertical axis wind turbines," *Energy*, vol. 180, pp. 838–857, 2019, doi: 10.1016/j.energy.2019.05.053.

[42] L. Daróczy, G. Janiga, K. Petrasch, M. Webner, and D. Thévenin, "Comparative analysis of turbulence models for the aerodynamic simulation of H-Darrieus rotors," *Energy*, vol. 90, pp. 680–690, 2015.

[43] R. Howell, N. Qin, J. Edwards, and N. Durrani, "Wind tunnel and numerical study of a small vertical axis wind turbine," *Renew. energy*, vol. 35, no. 2, pp. 412–422, 2010.

[44] A. Untaroiu, H. G. Wood, P. E. Allaire, and R. J. Ribando, "Investigation of self-starting capability of vertical axis wind turbines using a computational fluid dynamics approach," *J. Sol. Energy Eng.*, vol. 133, no. 4, 2011.

[45] J. McNaughton, F. Billard, and A. Revell, "Turbulence modelling of low Reynolds number flow effects around a vertical axis turbine at a range of tip-speed ratios," *J. Fluids Struct.*, vol. 47, pp. 124–138, 2014.

[46] J. M. Edwards, L. Angelo Danao, and R. J. Howell, "Novel experimental power curve determination and computational methods for the performance analysis of vertical axis wind turbines," *J. Sol. Energy Eng.*, vol. 134, no. 3, 2012.

[47] K. M. Almohammadi, D. B. Ingham, L. Ma, and M. Pourkashanian, "Modeling dynamic stall of a straight blade vertical axis wind turbine," *J. Fluids Struct.*, vol. 57, pp. 144–158, 2015.

[48] A. Arab, M. Javadi, M. Anbarsooz, and M. Moghiman, "A numerical study on the aerodynamic performance and the self-starting characteristics of a Darrieus wind turbine considering its moment of inertia," *Renew. Energy*, vol. 107, pp. 298–311, 2017.

[49] F. Balduzzi, J. Drofelnik, A. Bianchini, G. Ferrara, L. Ferrari, and M. S. Campobasso, "Darrieus wind turbine blade unsteady aerodynamics: a three-dimensional Navier-Stokes CFD assessment," *Energy*, vol. 128, pp. 550–563, 2017.

[50] H. F. Lam and H. Y. Peng, "Study of wake characteristics of a vertical axis wind turbine by two-and three-dimensional computational fluid dynamics simulations," *Renew. Energy*, vol. 90, pp. 386–398, 2016.

[51] M. Raciti Castelli, A. Englaro, and E. Benini, "The Darrieus wind turbine: Proposal for a new performance prediction model based on CFD," *Energy*, vol. 36, no. 8, pp. 4919–4934, 2011, doi: 10.1016/j.energy.2011.05.036.

[52] A. M. Biadgo, A. Simonović, D. Komarov, and S. Stupar, "Numerical and analytical investigation of vertical axis wind turbine," *FME Trans.*, vol. 41, no. 1, pp. 49–58, 2013.

[53] P. Sabaeifard, H. Razzaghi, and A. Forouzandeh, "Determination of Vertical Axis Wind Turbines Optimal Configuration through CFD Simulations," *2012 Int. Conf. Futur. Environ. Energy*, vol. 28, pp. 109–113, 2012.

[54] R. Gupta and A. Biswas, "Computational fluid dynamics analysis of a twisted three-bladed H-Darrieus rotor," *J. Renew. Sustain. Energy*, vol. 2, no. 4, 2010, doi: 10.1063/1.3483487.

[55] C. J. Simão Ferreira, H. Bijl, G. Van Bussel, and G. Van Kuik, "Simulating Dynamic Stall in a 2D VAWT: Modeling strategy, verification and validation with Particle Image Velocimetry data," *J. Phys. Conf. Ser.*, vol. 75, no. 1, 2007, doi: 10.1088/1742-6596/75/1/012023.

[56] I. B. Fridleifsson and D. H. Freeston, "Geothermal energy research and development," *Geothermics*, vol. 23, no. 2, pp. 175–214, 1994, doi: 10.1016/0375-6505(94)90037-X.

[57] "Solution Methods Applied Computational Fluid Dynamics. Lecture 5 - online presentation." https://en.ppt-online.org/648148 (accessed Apr. 30, 2022).

[58] B. Hanso, 済無*No Title No Title No Title*, vol. 4. 2016.

[59] S. W. Levy, *Use of Madribon in Dermatological Conditions, With Special Reference To Acne*, vol. 82, no. 1. 1959.

[60] A. Ismail-Zadeh and P. Tackley, *Computational methods for geodynamics*. Cambridge University Press, 2010.

[61] H. Beri and Y. Yao, "Effect of camber airfoil on self starting of Vertical Axis Wind Turbine.," *J. Environ. Sci. Technol.*, vol. 4, no. 3, pp. 302–312, 2011.

[62] I. Gökalp and E. Lebas, "Alternative fuels for industrial gas turbines (AFTUR)," *Appl.*

Therm. Eng., vol. 24, no. 11–12, pp. 1655–1663, 2004, doi: 10.1016/j.applthermaleng.2003.10.035.

[63] "The Cp-lamda curve." http://mstudioblackboard.tudelft.nl/duwind/Wind energy online reader/Static_pages/Cp_lamda_curve.htm (accessed May 21, 2022).

[64] "Wind energy technology." https://www.slideshare.net/taralsoliya/wind-energy-technology-70224162 (accessed May 26, 2022).

[65] C. A. Bustamante, W. F. Florez, H. Power, and A. F. Hill, "Hydrokinetic turbine location analysis by a local collocation method with Radial Basis Functions for two-dimensional Shallow Water equations," *WIT Trans. Ecol. Environ.*, vol. 195, pp. 3–13, 2015, doi: 10.2495/ESUS150011.

[66] H.-J. Bungartz and M. Schäfer, *Fluid-structure interaction: modelling, simulation, optimisation*, vol. 53. Springer Science & Business Media, 2006.

[67] Y. Bazilevs, K. Takizawa, and T. E. Tezduyar, *Computational fluid-structure interaction: methods and applications*. John Wiley & Sons, 2013.

[68] "Introduction — UW Libraries." https://www.lib.washington.edu/specialcollections/collections/exhibits/tnb (accessed Apr. 17, 2022).

[69] G. Hou, J. Wang, and A. Layton, "Numerical methods for fluid-structure interaction - A review," *Commun. Comput. Phys.*, vol. 12, no. 2, pp. 337–377, 2012, doi: 10.4208/cicp.291210.290411s.

[70] T. S. K. Goud, A. S. Kumar, and S. S. Prasad, "Analysis of fluid-structure interaction on an aircraft wing." Analysis, 2014.

[71] M. Rashed, S. Camporeale, M. Torresi, R. Bravo, S. Tullis, and S. Ziada, "Performance Testing of a Small Vertical-Axis Wind Turbine.pdf Related papers Experiment al result s of a vert ical axis wind t urbine Performance Testing of a Small Vertical-Axis Wind Turbine."

[72] J. H. Ferziger, M. Peric, and A. Leonard, "Computational Methods for Fluid Dynamics Table of Contents," *Phys. Today*, vol. 50, no. 3, p. 80, 1997, [Online]. Available: http://scitation.aip.org/content/aip/magazine/physicstoday/article/50/3/10.1063/1.881751.

[73] J. Blazek, *Computational fluid dynamics: principles and applications*. Butterworth-Heinemann, 2015.

[74] "NACA 0015 (naca0015-il)." http://airfoiltools.com/airfoil/details?airfoil=naca0015-il

(accessed Apr. 17, 2022).

[75] "NACA airfoil - Wikipedia." https://en.wikipedia.org/wiki/NACA_airfoil#Equation_for_a_symmetrical_4-digit_NACA_airfoil (accessed Apr. 17, 2022).

[76] M. R. Castelli, S. De Betta, and E. Benini, "Effect of blade number on a straight-bladed vertical-axis Darreius wind turbine," *World Acad. Sci. Eng. Technol.*, vol. 61, pp. 305–3011, 2012.

[77] R. Langtry, J. Gola, and F. Menter, "Predicting 2D airfoil and 3D wind turbine rotor performance using a transition model for general CFD codes," in *44th AIAA aerospace sciences meeting and exhibit*, 2006, p. 395.

[78] F. R. Menter, M. Kuntz, and R. Langtry, "Ten years of industrial experience with the SST turbulence model," *Turbul. heat mass Transf.*, vol. 4, no. 1, pp. 625–632, 2003.

[79] S. Meshes, "g Reference Introduction to," no. December, pp. 1–35, 2010.

[80] A. Fluent and A. F.- Ent, "Chapter 11 . Modeling Flows Using Sliding and Deforming Meshes."

[81] Inc. ANSYS, "L t 4 Lecture 4 Cell Zones and Boundary Conditions," no. December, pp. 1–22, 2010, [Online]. Available: http://imechanica.org/files/fluent_13.0_lecture04-boundary-conditions.pdf.

[82] "ANSYS FLUENT 12.0 User's Guide - 11.2.3 Solution Strategies for Sliding Meshes." https://www.afs.enea.it/project/neptunius/docs/fluent/html/ug/node392.htm (accessed Apr. 17, 2022).

[83] J. D. Anderson, *Introduction to Flight: 8th Edition*. 2016.

[84] S. Lain and C. Osorio, "Simulation and evaluation of a straight-bladed darrieus-type cross flow marine turbine," *J. Sci. Ind. Res. (India).*, vol. 69, no. 12, pp. 906–912, 2010.

[85] E. Vaishnav, "An Investigation on the Aerodynamic Performance of a Vertical Axis Wind Turbine," *Eng. Geol.*, vol. 104, pp. 144–155, 2010.

[86] ANSYS Fluent Tutorial Guide 18, "ANSYS Fluent Tutorial Guide 18," *ANSYS Fluent Tutor. Guid. 18*, vol. 15317, no. April, pp. 724–746, 2018.

[87] S. Islam and M. Z. R. Khan, "A Review of Energy Sector of Bangladesh," *Energy Procedia*, vol. 110, no. December 2016, pp. 611–618, 2017, doi: 10.1016/j.egypro.2017.03.193.

[88] A. Namiranian, "3D Simulation of a 5MW Wind Turbine," *Bth.Se*, p. 72, 2011, [Online].

Available:

http://www.bth.se/fou/cuppsats.nsf/all/b44c88bc0b99a4d7c1257940005d65db/$file/BTH201

2.Namiranian.pdf.